

Laboratory and Field Testing of an Accelerated Bridge Construction Demonstration Bridge: US Highway 6 Bridge over Keg Creek



Final Report
April 2013



IOWA STATE UNIVERSITY
Institute for Transportation

Sponsored by
Federal Highway Administration
Iowa Department of Transportation
(InTrans Project 11-411)

About the BEC

The mission of the Bridge Engineering Center is to conduct research on bridge technologies to help bridge designers/owners design, build, and maintain long-lasting bridges.

Disclaimer Notice

The contents of this report reflect the views of the authors, who are responsible for the facts and the accuracy of the information presented herein. The opinions, findings and conclusions expressed in this publication are those of the authors and not necessarily those of the sponsors.

The sponsors assume no liability for the contents or use of the information contained in this document. This report does not constitute a standard, specification, or regulation.

The sponsors do not endorse products or manufacturers. Trademarks or manufacturers' names appear in this report only because they are considered essential to the objective of the document.

Non-Discrimination Statement

Iowa State University does not discriminate on the basis of race, color, age, religion, national origin, sexual orientation, gender identity, genetic information, sex, marital status, disability, or status as a U.S. veteran. Inquiries can be directed to the Director of Equal Opportunity and Compliance, 3280 Beardshear Hall, (515) 294-7612.

Iowa Department of Transportation Statements

Federal and state laws prohibit employment and/or public accommodation discrimination on the basis of age, color, creed, disability, gender identity, national origin, pregnancy, race, religion, sex, sexual orientation or veteran's status. If you believe you have been discriminated against, please contact the Iowa Civil Rights Commission at 800-457-4416 or Iowa Department of Transportation's affirmative action officer. If you need accommodations because of a disability to access the Iowa Department of Transportation's services, contact the agency's affirmative action officer at 800-262-0003.

The preparation of this report was financed in part through funds provided by the Iowa Department of Transportation through its "Second Revised Agreement for the Management of Research Conducted by Iowa State University for the Iowa Department of Transportation" and its amendments.

The opinions, findings, and conclusions expressed in this publication are those of the authors and not necessarily those of the Iowa Department of Transportation or the U.S. Department of Transportation Federal Highway Administration.

Technical Report Documentation Page

1. Report No. InTrans Project 11-411		2. Government Accession No.		3. Recipient's Catalog No.	
4. Title and Subtitle Laboratory and Field Testing of an Accelerated Bridge Construction Demonstration Bridge: US Highway 6 Bridge over Keg Creek				5. Report Date April 2013	
				6. Performing Organization Code	
7. Author(s) Brent Phares, Jon "Matt" Rouse, and Jacob Miksell				8. Performing Organization Report No. InTrans Project 11-411	
9. Performing Organization Name and Address Bridge Engineering Center Iowa State University 2711 South Loop Drive, Suite 4700 Ames, IA 50010-8664				10. Work Unit No. (TRAIS)	
				11. Contract or Grant No.	
12. Sponsoring Organization Name and Address Iowa Department of Transportation 800 Lincoln Way Ames, IA 50010				13. Type of Report and Period Covered Final Report	
				14. Sponsoring Agency Code SPR 90-00-RB02-012	
15. Supplementary Notes Visit www.intrans.iastate.edu for color pdfs of this and other research reports.					
16. Abstract <p>The US Highway 6 Bridge over Keg Creek outside of Council Bluffs, Iowa is a demonstration bridge site chosen to put into practice newly-developed Accelerated Bridge Construction (ABC) concepts. One of these new concepts is the use of prefabricated high-performance concrete (HPC) bridge elements that are connected, in place, utilizing advanced material closure-pours and quick-to-install connection details.</p> <p>The Keg Creek Bridge is the first bridge in the US to utilize moment-resisting ultra-high performance concrete (UHPC) joints in negative moment regions over piers. Through laboratory and live load field testing, performance of these transverse joints as well as global bridge behavior is quantified and examined. The effectiveness of the structural performance of the bridge is evaluated to provide guidance for future designs of similar bridges throughout the US.</p>					
17. Key Words accelerated bridge construction—bond testing—bridge design evaluation— differential displacement—structural performance—transverse joints—ultra high- performance concrete—UHPC joints				18. Distribution Statement No restrictions.	
19. Security Classification (of this report) Unclassified.		20. Security Classification (of this page) Unclassified.		21. No. of Pages 59	22. Price NA

LABORATORY AND FIELD TESTING OF AN ACCELERATED BRIDGE CONSTRUCTION DEMONSTRATION BRIDGE: US HIGHWAY 6 BRIDGE OVER KEG CREEK

Final Report
April 2013

Principal Investigator
Brent Phares, Director
Bridge Engineering Center, Iowa State University

Co-Principal Investigator
Jon “Matt” Rouse, Assistant Professor
Civil, Construction, and Environmental Engineering, Iowa State University

Research Assistant
Jacob Miksell

Authors
Brent Phares, Jon “Matt” Rouse, and Jacob Miksell

Sponsored by
the Iowa Department of Transportation
and the Federal Highway Administration
State Planning and Research Funding
(SPR 90-00-RB02-012)

Preparation of this report was financed in part
through funds provided by the Iowa Department of Transportation
through its research management agreement with the
Institute for Transportation
(InTrans Project 11-411)

A report from
Institute for Transportation
Iowa State University
2711 South Loop Drive, Suite 4700
Ames, IA 50010-8664
Phone: 515-294-8103 Fax: 515-294-0467
www.intrans.iastate.edu

TABLE OF CONTENTS

ACKNOWLEDGMENTS	ix
EXECUTIVE SUMMARY	xi
Background.....	xi
Research Description	xi
Key Findings.....	xi
Implementation Benefits and Readiness.....	xii
1 INTRODUCTION	1
2 BRIDGE DESCRIPTION.....	2
3 BOND TESTING.....	3
3.1 Methods.....	3
3.2 Results and Discussion	10
4 FIELD TESTING.....	12
4.1 Instrumentation and Test Methodology	12
4.2 Live Load Test Results	17
5 CONCLUSIONS.....	43
5.1 Bond Testing.....	43
5.2 Design Assumptions	44
5.3 Maximum Bridge Strains and Displacements.....	44
5.4 Comparison of 2011 and 2012 Pseudo-Static Live Load Tests.....	44
REFERENCES	47
BIBLIOGRAPHY.....	47

LIST OF FIGURES

Figure 2.1. Bridge plan view.....	2
Figure 2.2. Bridge cross-section view.....	2
Figure 3.1. Direct tension test specimen.....	4
Figure 3.2. Direct tension test half-specimen connection.....	4
Figure 3.3. Direct tension test precast concrete half-specimen jig	5
Figure 3.4. Direct tension test UHPC half-specimen jig	5
Figure 3.5. Direct tension setup	6
Figure 3.6. Pressure-washed test specimen.....	7
Figure 3.7. Sandblasted and grooved test specimens.....	8
Figure 3.8. Epoxy-bonded test specimen	8
Figure 3.9. Simulated MOR specimen.....	9
Figure 3.10. Pressure-washed test specimens	9
Figure 3.11. Sandblasted and grooved test specimens.....	10
Figure 4.1. Instrumentation plan view	12
Figure 4.2. Transverse joint instrumentation plan view and embedded gauge labels	13
Figure 4.3. Transverse joint instrumentation section view and surface-mounted gauge grid lines.....	13
Figure 4.4. Instrumentation layout of surface-mounted gauges on girders at midspan and load paths	14
Figure 4.5. Instrumentation layout at east pier	16
Figure 4.6. Test truck configuration and loading.....	17
Figure 4.7. Representative data from load path 3 of 2011 live load strains of top of deck gauges south line.....	19
Figure 4.8. Representatvie data from load path 3 of 2011 live load strains of top of deck gauges north line	19
Figure 4.9. Representative data from load path 3 of 2011 live load strains of bottom of deck gauges south line.....	20
Figure 4.10. Representative data from load path 3 of 2011 live load strains of bottom of deck gauges north line	20
Figure 4.11. Comparison of live load strains from 2011 to 2012 of surface-mounted transducers spanning interface load path 2	23
Figure 4.12. Comparison of live load strains from 2011 to 2012 of surface-mounted transducers away from interface load path 2	23
Figure 4.13. Observed cracking at instrumented joint at location of ToD N 4 transducer	25
Figure 4.14. Observed cracking of longitudinal joint between modules 2 and 3	25
Figure 4.15. Observed efflorescence between modules 2 and 3 on bottom of deck.....	26
Figure 4.16. Close-up of cracking and efflorescence observed between module 2 and 3 on bottom of deck	26
Figure 4.17. Representative data from load path 4 of 2011 live load strains for steel girders of modules 3 and 4 at midspan	29
Figure 4.18. Representative data from load path 4 of 2011 live load strains for steel girders of modules 1 and 2 at midspan	29
Figure 4.19. Representative data from load path 3 of 2011 live load strains for steel girders of module 3 at abutment	32

Figure 4.20. Representative data from load path 3 of 2011 live load strains for steel girders of module 3 at pier	32
Figure 4.21 Comparison of live load strains from 2011 to 2012 of transducers on bottom flange of girder at midspan for module 3 from load path 4	35
Figure 4.22. Comparison of live load strains from 2011 to 2012 of transducers on top flange of girder at midspan for module 3 from load path 4	35
Figure 4.23. Comparison of live load strains from 2011 to 2012 of transducers on bottom flange of girder at abutment for module 3 from load path 3.....	38
Figure 4.24. Comparison of live load strains from 2011 to 2012 of transducers on bottom flange of girder at pier for module 3 from load path 3	39
Figure 4.25. Comparison of live load strains of pier cap.....	41

LIST OF TABLES

Table 3.1. Precast concrete-HPC interface bond testing variables	7
Table 3.2. Direct tension and MOR testing results	11
Table 4.1. Transverse joint surface-mounted transducer nomenclature	14
Table 4.2. Girder transducer nomenclature.....	15
Table 4.3. 2011 Maximum live load strains ($\mu\epsilon$) of top of deck surface-mounted gauges at transverse joint	18
Table 4.4. 2011 Maximum live load strains ($\mu\epsilon$) of bottom of deck surface-mounted gauges at transverse joint	18
Table 4.5. 2011 Maximum live load strains ($\mu\epsilon$) of embedded gauges at transverse joint	18
Table 4.6. 2012 Normalized maximum live load strains ($\mu\epsilon$) of top of deck surface-mounted gauges at transverse joint	21
Table 4.7. 2012 Normalized maximum live load strains ($\mu\epsilon$) of bottom of deck surface-mounted gauges at transverse joint	22
Table 4.8. 2012 Normalized maximum live load strains ($\mu\epsilon$) of embedded gauges at transverse joint	22
Table 4.9. Live load strain difference from 2011 test to 2012 test top of deck transducers load path 2.....	23
Table 4.10. 2011 Maximum live load strains ($\mu\epsilon$) of bottom flange of steel girders at midspan..	27
Table 4.11. 2011 Maximum live load strains ($\mu\epsilon$) of top flange of steel girders at midspan	28
Table 4.12. 2011 Load fractions and distribution factors	30
Table 4.13. 2011 Maximum live load strains ($\mu\epsilon$) of bottom flange of steel girders at abutment.....	31
Table 4.14. 2011 Maximum live load strains ($\mu\epsilon$) of bottom flange of steel girders at pier	31
Table 4.15. 2012 Normalized maximum live load strains ($\mu\epsilon$) of bottom flange of steel girders at midspan	33
Table 4.16. 2012 Normalized maximum live load strains ($\mu\epsilon$) of top flange of steel girders at midspan.....	33
Table 4.17. 2012 Maximum differential deflection at midspan.....	34
Table 4.18. Live load strain difference from 2011 test to 2012 test of bottom flange transducer on girder at midspan for module 3 from load path 4	35
Table 4.19. Live load strain difference from 2011 test to 2012 test of top flange transducer on girder at midspan for module 3 from load path 4	36
Table 4.20. 2012 Load fractions and distribution factors	36
Table 4.21. Comparison of 2011 and 2012 distribution factors	37
Table 4.22. 2012 Normalized maximum live load strains ($\mu\epsilon$) of bottom flange of steel girders at abutment.....	37
Table 4.23. 2012 Normalized maximum live load strains ($\mu\epsilon$) of bottom flange of steel girders at pier	38
Table 4.24. 2011 Maximum strains of pier cap	40
Table 4.25. 2012 Normalized maximum live load strains ($\mu\epsilon$) of pier cap	40
Table 4.26. 2011 Maximum deflections at pier cap to column interface	41
Table 4.27. 2012 Maximum deflections at pier cap to column interface	42

ACKNOWLEDGMENTS

The authors would like to thank the Office of Bridges and Structures at the Iowa Department of Transportation (DOT) for sponsoring this research and the Federal Highway Administration for state planning and research (SPR) funds used for this project.

EXECUTIVE SUMMARY

Background

To address the need for the development of a fast, repeatable, and dependable way to replace “typical” bridges across the country, the Transportation Research Board (TRB) developed project R04, Innovative Designs for Rapid Renewal, as part of the Second Strategic Highway Research Program (SHRP 2). The goal of this project was to develop standardized accelerated bridge construction (ABC) systems for nationwide use (Iowa DOT Office of Bridges and Structures 2011).

As part of the SHRP 2 Project R04, the Iowa Department of Transportation (DOT) was asked to select a demonstration bridge site to implement some of the ABC design concepts being developed.

The Iowa DOT selected a replacement bridge site in western Iowa on US Highway 6 over Keg Creek in Pottawattamie County. This site was selected due to the abundance of similar three-span bridges in Iowa and many other states. Bridge engineers wanted to ensure that what was learned from the R04 project would be applicable to future bridge projects (Iowa DOT Office of Bridges and Structures 2011).

Research Description

The basic ABC concept employed in the Keg Creek Bridge project was to utilize prefabricated elements that are connected, in place, utilizing advanced material closure-pours and quick-to-install connection details.

First, it was desired to know more about the bond performance between the concrete deck high-performance concrete (HPC) and the closure pour material, ultra-high performance concrete (UHPC). Second, it was desired to understand how the completed bridge performed from a global and local perspective.

To answer the first question, a series of laboratory tests were conducted. To answer the second question, two live load tests were conducted on the completed bridge with one immediately following construction and one approximately seven months later.

Key Findings

As the bridge was being designed, simultaneous laboratory testing was being performed at Iowa State University of these transverse joints to be used. The results of these tests indicated special attention needed to be paid at these locations due to insufficient bond strength between the HPC and UHPC.

Through further laboratory testing of the bond strength at the HPC/UHPC interface, it is clear that there was cause for concern of opening at these interfaces. These concerns were reinforced by the findings in the comparison of the live load field tests.

Visual inspection, as well as evaluation of the collected data, showed a breakdown of the bond between the interface of the HPC and UHPC at the joints. The breakdown of this bond resulted in cracking of the deck allowing an ingress of road salts, which is verified by the presence of efflorescence on the underside of the bridge deck at joint interfaces.

Furthermore, the live load field testing was also used to quantify and compare global bridge behavior over a period of approximately seven months. The overall behavior of the bridge was very similar from test to test with the exception of the breakdown of bond at the joint interfaces.

Implementation Benefits and Readiness

The use of moment-resisting transverse UHPC joints at pier locations in the Keg Creek Bridge was a first for the US and is one of many concepts being employed to reduce road closure time as part of the development of ABC practices to be used throughout the country. Utilizing these technologies, road closure was reduced from an entire construction season to only two weeks.

1 INTRODUCTION

As a result of an aging infrastructure throughout the US, a need has arisen for the development of a fast, repeatable, and dependable way to replace “typical” bridges across the country. To address this need, the Transportation Research Board (TRB) developed project R04, Innovative Designs for Rapid Renewal, as part of the Second Strategic Highway Research Program (SHRP 2). The goal of this project was to develop standardized accelerated bridge construction (ABC) systems for nationwide use (Iowa DOT Office of Bridges and Structures 2011).

As part of the SHRP 2 Project R04, the Iowa Department of Transportation (DOT) was asked to select a demonstration bridge site to implement some of the ABC design concepts being developed. The Iowa DOT selected a replacement bridge site in western Iowa on US Highway 6 over Keg Creek in Pottawattamie County. This site was selected due to the abundance of similar three-span bridges in Iowa and many other states. Bridge engineers wanted to ensure that what was learned from the R04 project would be applicable to future bridge projects (Iowa DOT Office of Bridges and Structures 2011).

The basic ABC concept employed in the Keg Creek Bridge project was to utilize prefabricated elements that are connected, in place, utilizing advanced material closure-pours and quick-to-install connection details. Utilizing these technologies, road closure was reduced from an entire construction season to only two weeks.

This report documents testing completed to answer several design questions. First, it was desired to know more about the bond performance between the concrete deck high-performance concrete (HPC) and the closure pour material, ultra-high performance concrete (UHPC). Second, it was desired to understand how the completed bridge performed from a global and local perspective.

To answer the first question, a series of laboratory tests were conducted. To answer the second question, two live load tests were conducted on the completed bridge with one immediately following construction and one approximately seven months later.

This report is divided into five chapters. Chapter 2 describes the specifications and features of the Keg Creek Bridge. Chapter 3 describes the bond testing completed in the laboratory at Iowa State University. The field testing is described in Chapter 4. Final conclusions are presented in Chapter 5.

2 BRIDGE DESCRIPTION

The US Highway 6 Bridge over Keg Creek is located southeast of Council Bluffs, Iowa in Pottawattamie County. The demonstration bridge is designed to represent a “typical” ABC bridge whose standards and specifications can be used repeatedly throughout the US.

The new bridge is a three-span, 204 ft 6 in. (center of bearing to center of bearing) long by 47 ft 2 in. wide steel/precast modular structure. The bridge consists of two 67 ft 3 in. end spans with a 70 ft center span. These spans are supported at the pier locations by precast pier caps and columns connected through the use of grouted couplers. The demonstration bridge also utilized precast bridge approaches and semi-integral abutments to help reduce the construction time. The cross sections of the bridge spans are made up of six precast deck modules.

Each module is compositely constructed through the use of shear studs with two W30X99 steel beams supporting an 8.5 in. concrete deck. The exterior modules also have an integral guardrail running the length of the bridge. Modules were connected on-site through the utilization of full depth longitudinal and transverse moment-resisting joints infilled with UHPC. The use of these moment-resisting UHPC joints at the piers is a first in the US. Plan and cross-section views of the bridge can be found in Figure 2.1 and Figure 2.2, respectively.

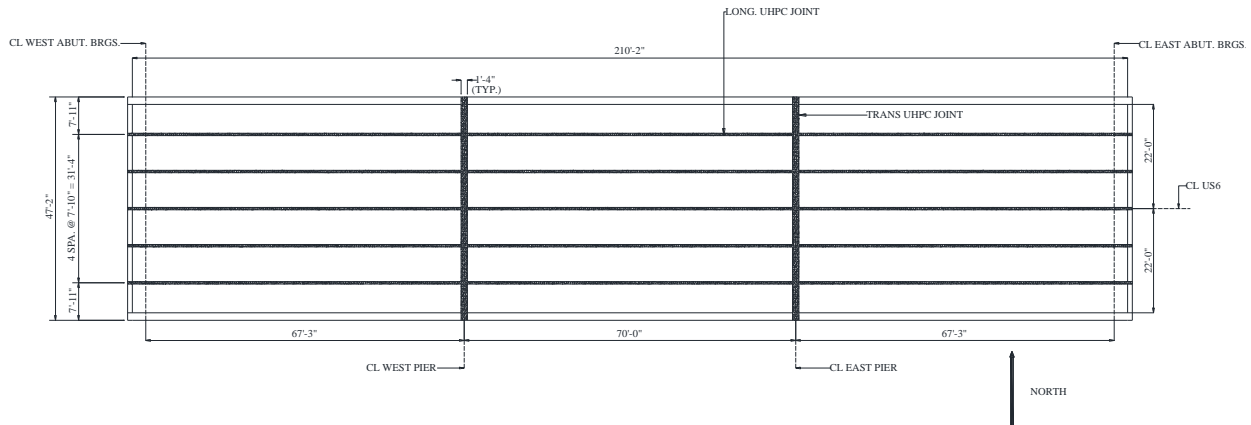


Figure 2.1. Bridge plan view

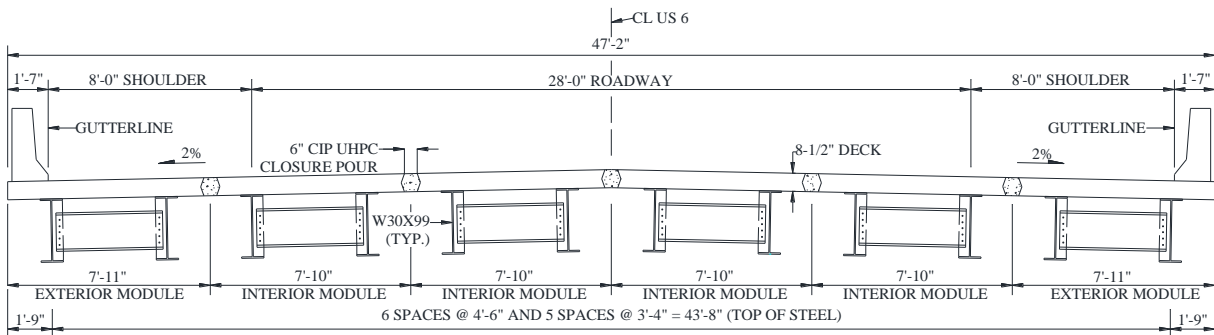


Figure 2.2. Bridge cross-section view

3 BOND TESTING

The interface between the precast deck panels and cast-in-place UHPC used in joining the precast decks of the SHRP 2 – R04 accelerated construction project is an obvious location of concern for ingress of water and chlorides. The tensile bond strength between precast concrete bridge decks and UHPC joints will be an important factor in the longer-term durability of any bridge using this type of full depth deck joint detail. To assess the strength of this bond and identify important parameters affecting the bond strength, two series of tests were conducted. The laboratory tests conducted and their objectives follow:

- Test Type 1: Direct Tension Testing
 - The first suite of tests measures the bond strength in direct tension
- Test Type 2: Simulated Modulus of Rupture (MOR) Testing
 - The second suite of tests, mimicking a modulus of rupture test, measures the lower bound of strength between concrete fracture and bond failure

3.1 Methods

3.1.1 Test Type 1: Direct Tension Testing

The first set of tests measured the bond strength in direct tension. While there is an ASTM standard (ASTM C1583 / C1583M – 04e1 Standard Test Method for Tensile Strength of Concrete Surfaces and the Bond Strength or Tensile Strength of Concrete Repair and Overlay Materials by Direct Tension (Pull-off Method)) for measuring tensile bond, this test is intended for overlays and can only quantify the weaker of the bond or the tensile strength of the underlying concrete. Several tests procedures have been proposed to measure the direct tensile strength of unreinforced concrete, but all present difficulties in alignment, concentricity, and uniformity of stress conditions. The results of such tests are often very sensitive to workmanship and procedure.

To test the direct tensile bond strength in this work, 4 in. diameter cylinders of concrete were cast with a threaded steel rod throughout the entire length of the half-specimen. Then, the second half of the specimen was match-cast onto the precast concrete half, again with a threaded rod through the length of the UHPC half-specimen as shown in Figure 3.1.

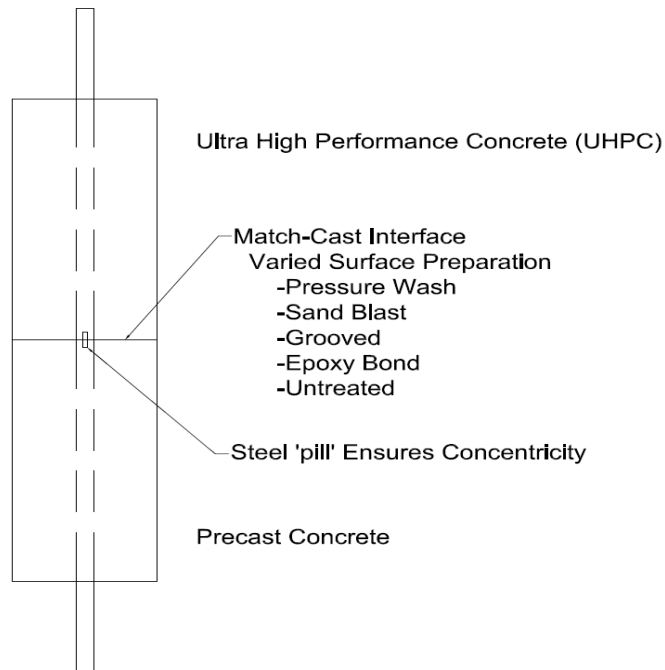


Figure 3.1. Direct tension test specimen

A steel “pill,” acting as a male connector between two machined holes in the threaded rods, helped ensure alignment of the threaded rods in each half-specimen (Figure 3.2).



Figure 3.2. Direct tension test half-specimen connection

Jigs were constructed to ensure alignment and concentricity during casting of the normal concrete half-specimens (Figure 3.3).



Figure 3.3. Direct tension test precast concrete half-specimen jig

Once the precast concrete half-specimens had received their specific surface finish and cured for 28 days, another jig was again used during match casting of the UHPC to ensure alignment and concentricity (Figure 3.4).



Figure 3.4. Direct tension test UHPC half-specimen jig

With specimens like those used in this work, unlike the ASTM C1583 procedure, failure was forced to occur at the interface to compute bond strength. Each specimen was tested in Iowa State University's MTS universal testing machine to ensure maximum concentricity and precise alignment. The specimen was secured in the MTS machine with friction grips using an eye bolt-to-connector-to-eye nut assembly (Figure 3.5). This connection assembly successfully eliminated eccentricities that could have been caused by directly gripping the specimens threaded rods with the MTS testing machine.



Figure 3.5. Direct tension setup

The objective of these tests was to quantify the effect of various surface preparations as well as the effect of UHPC maturity on direct tensile bond strength. Six different surface preparations were tested: pressure-washed at 1,500 psi, pressure-washed at 3,000 psi, sandblasted, groove-cut, epoxy-bonded, and untreated.

Once construction of the full specimens was complete, testing in the MTS universal testing machine took place four days after placement of the UHPC for the six surface finishes. The 1,500 psi pressure washed surface specimens were used to further assess the effect of UHPC maturity on the tensile bond strength. Those specimens were tested at 2, 4, 7, 14, and 28 days after UHPC placement. The epoxy bonding agent used for this test was Rezi-Weld™ 1000, from W. R. Meadows.

The testing plan for all direct tension testing specimens can be seen in Table 3.1. Figure 3.6 through Figure 3.8 display the surface preparations for the testing. Note that SSD in Table 3.1 indicates the specimen was prepared with a saturated surface dry (SSD) condition.

Table 3.1. Precast concrete-HPC interface bond testing variables

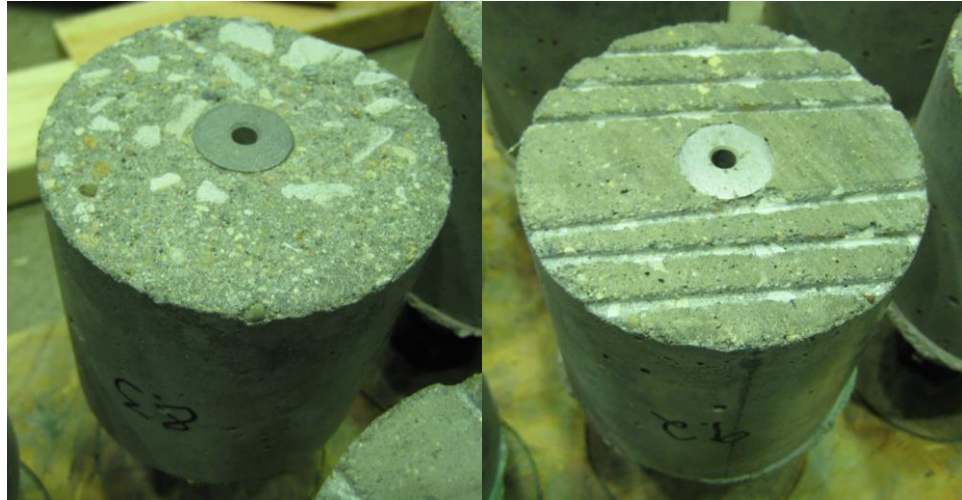
No. of Specimens	Interface Preparation	SSD	UHPC Age (days)
3	1,500 psi pressure wash	SSD	2
3	1,500 psi pressure wash	SSD	4
3	1,500 psi pressure wash	SSD	7
3	1,500 psi pressure wash	SSD	14
3	1,500 psi pressure wash	SSD	28
3	3,000 psi pressure wash	SSD	4
3	Plywood - untreated	SSD	4
3	Sandblasted	SSD	4
3	Groove cut	SSD	4
3	Epoxy bonding agent		4



(a) 1,500 psi

(b) 3,000 psi

Figure 3.6. Pressure-washed test specimen



(a) Sandblasted

(b) Grooved

Figure 3.7. Sandblasted and grooved test specimens



Figure 3.8. Epoxy-bonded test specimen

3.1.2 Test Type 2: Simulated Modulus of Rupture Testing

A second suite of tests that mimicked a modulus of rupture (ASTM C78 – Flexural Strength of Concrete) test was utilized as well. In this test setup, each half-beam specimen was cast of unreinforced concrete and allowed to cure. The second half of the beam was match-cast of UHPC with the interface at the centerline of the beam (Figure 3.9). The beam was then tested in three point bending to compute the stress at which the bond fails.

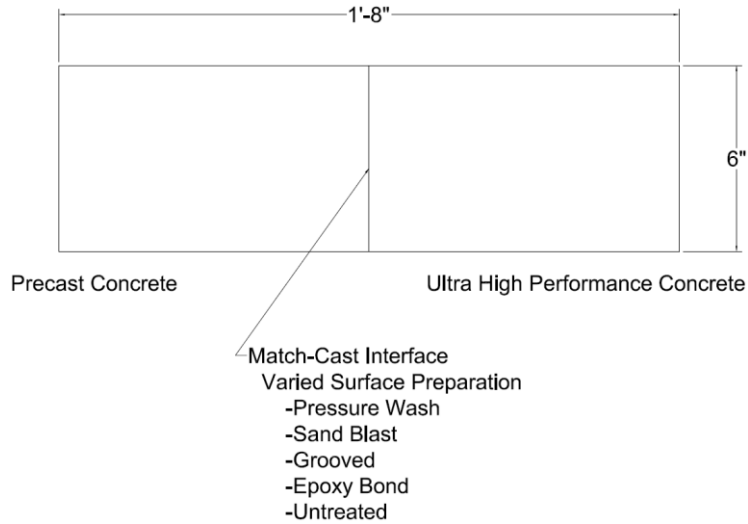
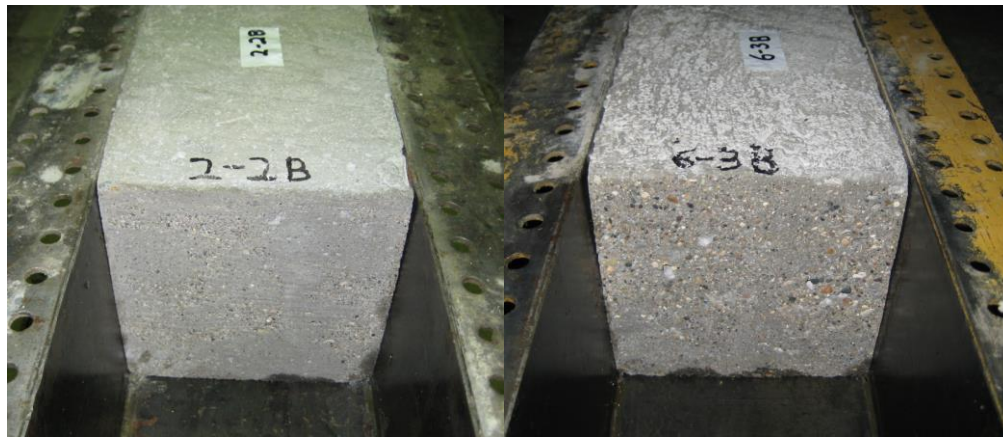


Figure 3.9. Simulated MOR specimen

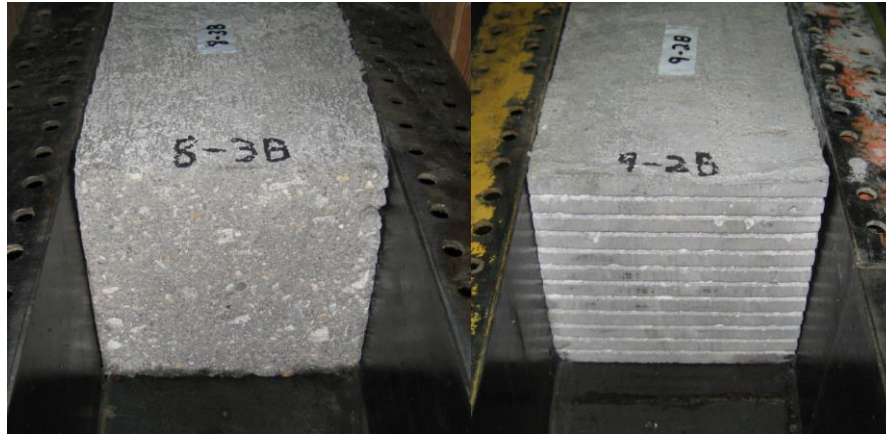
In these tests, the failure was not ensured to occur at the interface, and only a lower bound for bond strength may be computed if the concrete fractures before the bond fails. While such a test does not directly yield the tensile bond strength, the results would likely prove useful for comparison with the modulus of rupture of various concrete mixes. The interface surfaces in the beam specimens were prepared in the same fashion as for the direct tensile testing specimens, using the six different finishes. Simulated modulus of rupture testing was carried out in the same fashion as shown in Table 3.1. Various specimen surface finishes can be seen in Figure 3.10 and Figure 3.11.



(a) 1,500 psi

(b) 3,000 psi

Figure 3.10. Pressure-washed test specimens



(a) Sandblasted

(b) Grooved

Figure 3.11. Sandblasted and grooved test specimens

3.2 Results and Discussion

Presented in Table 3.2 are the results of both the direct tension and simulated MOR lab test results. Note first that if there is no preparation to the interface between the HPC/UHPC (plywood-untreated), there is virtually no bond between the two materials at all, indicating a necessity for some kind of surface preparation.

The most effective of the surface preparations tested in direct tension at the 4 day UHPC age appear to be the use of a 3,000 psi pressure wash or an epoxy bonding agent. The 3,000 psi pressure wash also performed comparatively well in the simulated MOR test, resulting in the only specimen that had a failure away from the interface. The epoxy bonding agent did not perform as well in the simulated MOR test, only outperforming the untreated interface preparation for a specimen with a UHPC age of 4 days. The MOR averages for all interface preparations were calculated to be below the estimated MOR for a 5,000 psi compressive strength HPC (as was used in the Keg Creek Bridge prefabricated elements) as calculated according to the American Concrete Institute (ACI) Building Code and Commentary 318-11 Equation 9-10 (~530 psi). The location of the bond is then the weakest point within the beam and therefore the most likely location for cracking to occur.

It seems that throughout the test data there is a rather large range between maximum and minimum values for bond strength of similar specimen in both tests. These differences are especially evident in the direct tension test. This shows a high degree of inconsistency in the bond strength between the HPC and UHPC, no matter the surface preparation.

It is evident that UHPC maturity also has an effect on the tensile bond strength. In both tests, the tensile bond strength increases up to the 7 day UHPC age where it peaks and then sees a drop in bond strength as it reaches its 14 and 28 day UHPC ages. This shows evidence of deterioration of the bond over time.

Therefore, even though the UHPC material itself gives advantages in both low permeability and increased strength, the bond of the material to that of precast HPC is of concern. Without a consistent method to improve this bond, the interface location will be at risk for ingress of road salts and chemicals that could corrode the internal reinforcement. This is especially a concern in the Keg Creek project, where the UHPC joints are used in a negative moment region.

Table 3.2. Direct tension and MOR testing results

Interface Preparation	UHPC Age (days)	Direct Tension (psi)			MOR (psi)		
		Average	Low	High	Average	Low	High
1,500 psi pressure wash	2	112	46	174	380	495	261
1,500 psi pressure wash	4	115	18	224	308	390	261
1,500 psi pressure wash	7	218	91	285	387	510	326
1,500 psi pressure wash	14	72	48	105	369	415	345
1,500 psi pressure wash	28	112	45	229	208	300	149
3,000 psi pressure wash	4	169	81	225	504	537	484
Plywood - untreated	4	9	8	9	26	39	19
Sandblasted	4	96	64	127	378	403	362
Groove cut	4	146	85	221	395	433	332
Epoxy bonding agent	4	211	196	224	267	315	228

4 FIELD TESTING

4.1 Instrumentation and Test Methodology

The Bridge Engineering Center (BEC), along with the Iowa DOT and HNTB, worked together to develop a plan for testing the US Highway 6 Bridge over Keg Creek in order to evaluate and quantify the behavior of the structure. This test plan consisted of monitoring both important strains and deflections through surface-mounted and embedded strain gauges along with string potentiometers.

During testing, a tandem-axle dump truck with known weight and dimensions (described subsequently) was driven slowly across the bridge to measure the effects of a known pseudo-static live load. The evaluation plan called for two separate tests conducted approximately 7 months apart. The first of these was performed in November 2011, shortly before the bridge was opened to traffic, and the second was performed in May 2012.

In each test, 58 surface-mounted strain transducers along with eleven embedded strain transducers were used to monitor the response of the bridge at locations deemed critical because of expected strain levels. A plan view of the instrumentation plan is shown in Figure 4.1.

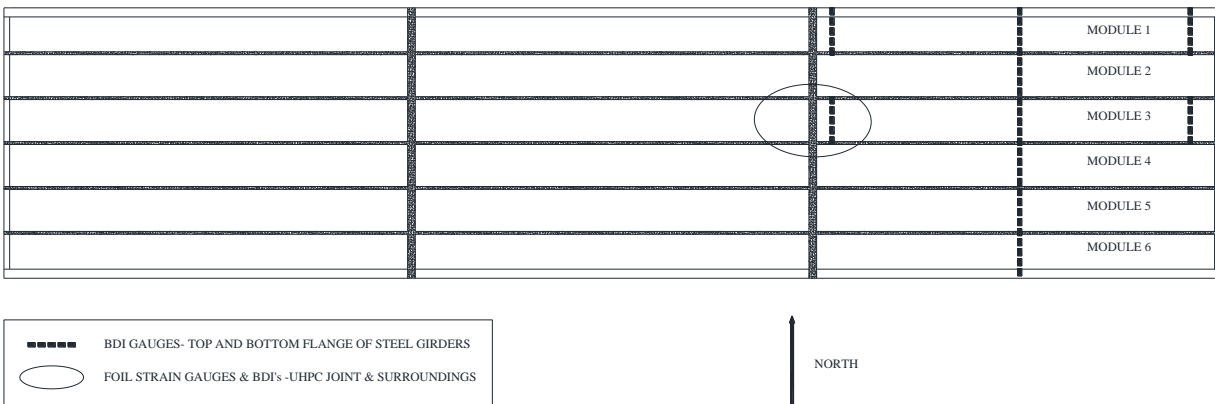


Figure 4.1. Instrumentation plan view

One of the most heavily instrumented areas of the test was the transverse joint between the east end span and the center span of the bridge at module 3. This negative moment region is the same as the joint that was the subject of much previous study (Rouse et al. 2011). At this location, 16 surface-mounted gauges were attached to the top and bottom of the deck along two rows located 14.5 in. inwards from the centerline of the longitudinal UHPC joints along the north and south of the module.

Ten gauges were mounted to the top of the deck, in two rows of five, at locations outside of the transverse joint, across the interface of the joint, and at the centerline of the joint. The other six surface-mounted gauges at the transverse joint were located on the bottom of the deck in two

rows of three with gauges spanning the interface of the joint and gauges at the centerline of the joint.

The eleven embedded strain gauges are also located at this transverse joint location along the same two rows as the surface-mounted gauges. Foil strain gauges were placed on the longitudinal bars 6 ft from the centerline of the UHPC joint, at the location of the termination of the hairpin lap splice, and on the hairpin bars at the location of the termination of the longitudinal lap splice. All of these locations are outside of the UHPC joint in the prefabricated deck panels.

The layout of the gauges located at the transverse joint and their labeling are shown in Figure 4.2 and Figure 4.3 with the naming key for surface-mounted transducers in Table 4.1.

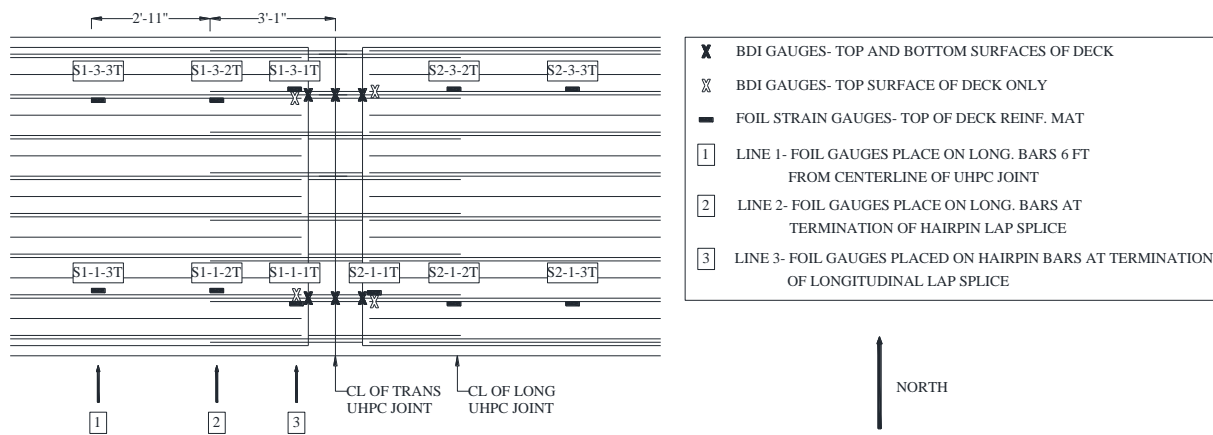


Figure 4.2. Transverse joint instrumentation plan view and embedded gauge labels

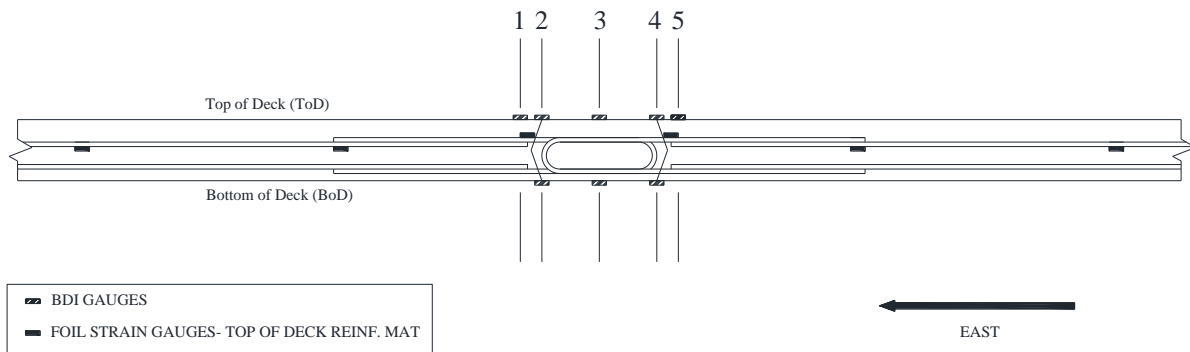


Figure 4.3. Transverse joint instrumentation section view and surface-mounted gauge grid lines

Table 4.1. Transverse joint surface-mounted transducer nomenclature

Elevation		North/South Grid line		East/West Grid Line	
ToD	Top of Deck	N	North Grid Line	1	Grid Line 1
BoD	Bottom of Deck	S	South Grid Line	2	Grid Line 2
				3	Grid Line 3
				4	Grid Line 4
				5	Grid Line 5

Example: ToD S 4=Top of Deck along South line at west interface of joint

Thirty-two of the 58 surface-mounted transducers were attached to the steel girders of the precast deck modules at the midspan, abutment, and pier locations of the east end span of the bridge. Every girder of the bridge was instrumented at the underside of the top and bottom flanges across the bridge at the midspan, while only the girders under the first and third module were instrumented at the pier and abutment locations. The layout of these surface-mounted gauges at midspan can be seen in Figure 4.4 with the naming key of all girder surface-mounted gauges found in Table 4.2.

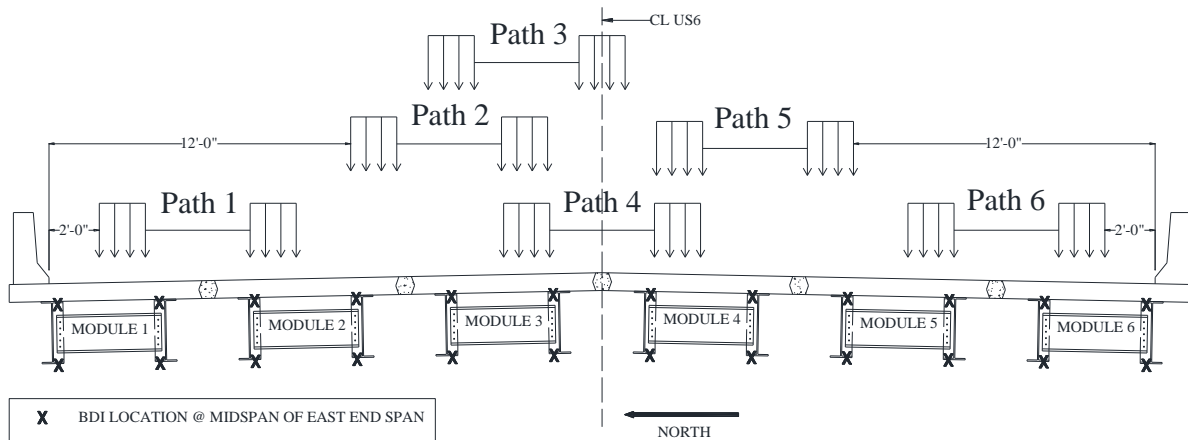


Figure 4.4. Instrumentation layout of surface-mounted gauges on girders at midspan and load paths

Table 4.2. Girder transducer nomenclature

Module #		Span Location		Location on X-section	
M1	Module 1	Mid	Midspan	BN	Bottom North
M2	Module 2	Abut	East Abutment	BS	Bottom South
M3	Module 3	Pier	East Pier	TN	Top North
M4	Module 4			TS	Top South
M5	Module 5				
M6	Module 6				

Example: M3 Abut BN=transducer on module 3 near the abutment on the bottom flange of the north module girder

Other critical locations chosen for instrumentation included near novel pier connection joints and at other important areas. To investigate the behavior of the piers, instrumentation was placed at strategic locations on the east pier. Two surface-mounted transducers were attached at midspan of the pier cap on the top and bottom surfaces to observe the global behavior. The east pier was also monitored with displacement transducers.

For the 2011 test, two string potentiometers were attached over the interface of the pier cap-to-column connection on the north column of the pier. Both potentiometers were mounted to the north face of the column with one on the east side and one on the west side. Instrumentation at this location was implemented to determine if any rocking of the pier cap in the longitudinal direction of the bridge was present.

For the second test, two more displacement transducers were included in addition to the two from the first test. The additional string potentiometers were mounted on the south face of the north column at the east pier to check for rocking of the pier cap in the transverse direction of the bridge also (Figure 4.5).

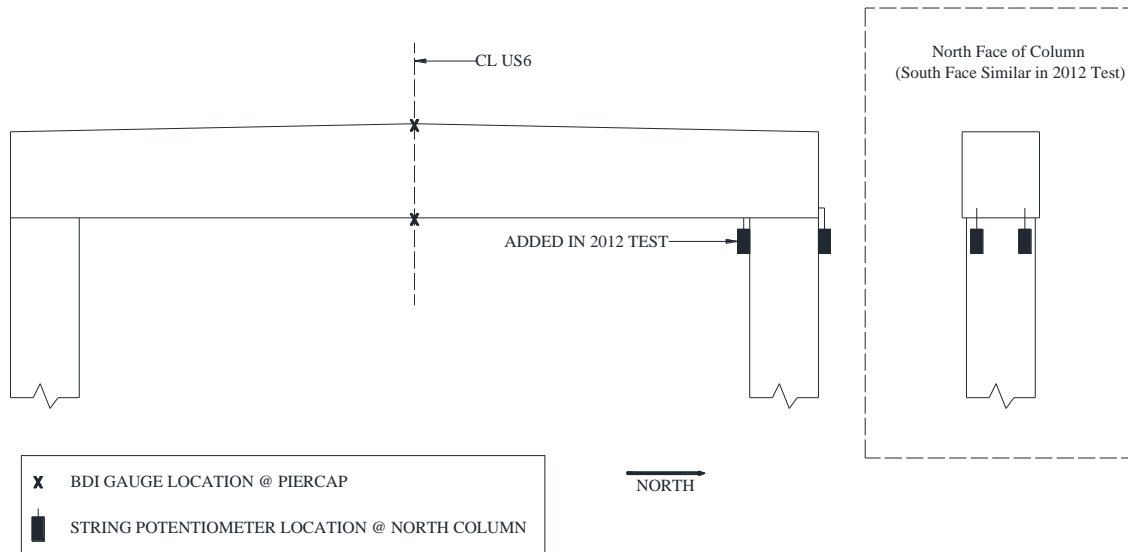


Figure 4.5. Instrumentation layout at east pier

Based on visual observation of the longitudinal joint, one string potentiometer was added to the 2012 instrumentation plan. This string potentiometer was located at the centerline of the bridge at midspan. This displacement transducer was added to check for any large differential displacements between the precast HPC deck and the UHPC longitudinal joint between modules 3 and 4.

As mentioned previously, both tests were performed by driving a three-axle truck across the bridge at a crawl speed (< 5 mph) from west to east. This process was executed twice for each of the six specified load paths to ensure repeatability of the data. The layout of all load paths can be seen in Figure 4.4. Paths 2 and 5 represent typical traffic locations along the center of each lane. Paths 1 and 6 are located two ft from the face of the guardrail. Path 4 represents the truck traversing the bridge while centered over the centerline of the bridge. Path 3 represents the truck traversing the bridge with its right tire centered on the centerline of the bridge.

The test vehicle consisted of a loaded three-axle dump truck. The 2011 test truck was loaded to a weight of 70,700 lbs, while the 2012 test truck had a weight of 52,160 lbs. Due to this fact, all data from the 2012 test was multiplied by a normalization factor of 1.355 to adjust for the differing weights in an attempt to ease comparative interpretations. Test truck configuration and weights for the two trucks are shown in Figure 4.6.

Starting and ending points for runs also varied between the two tests. Note that in all graphs involving truck position, the data are presented with respect to the front axle position. A truck position of zero represents when the front axle is at the west bridge joint.

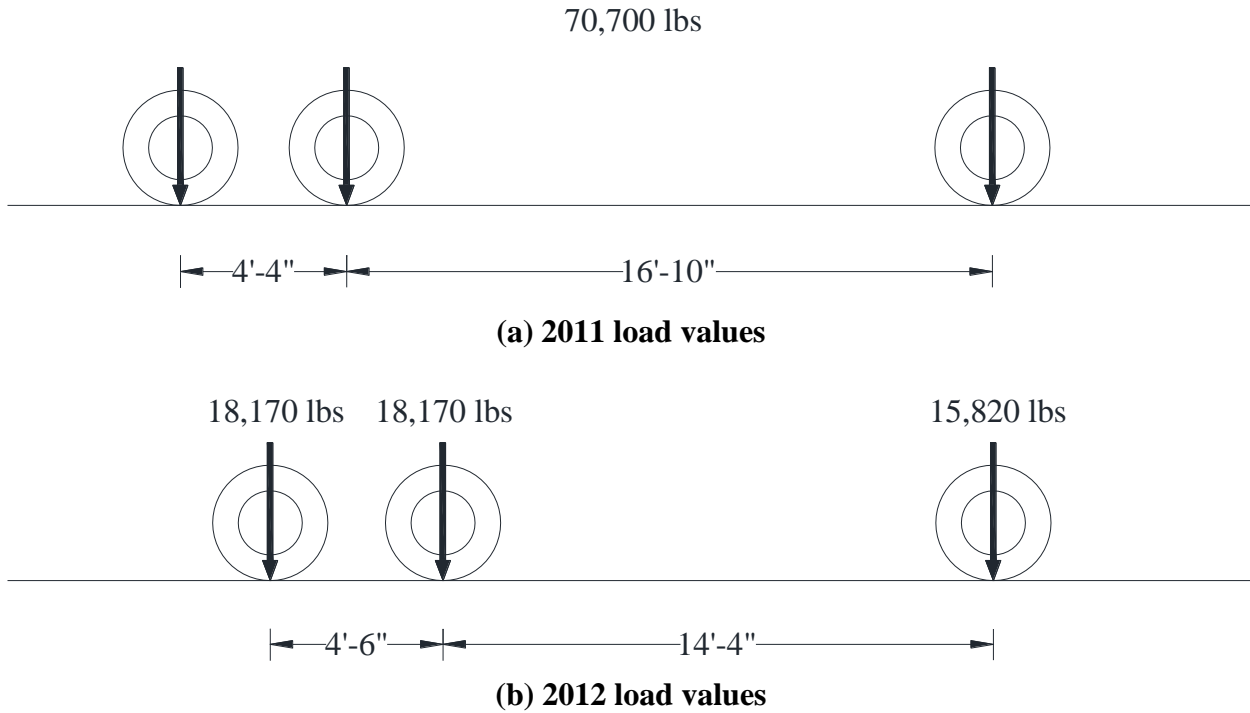


Figure 4.6. Test truck configuration and loading

4.2 Live Load Test Results

In this section, results are presented for the pseudo-static live load tests performed on the US Highway 6 Bridge over Keg Creek in both November 2011 and May 2012. For each test, the six specified load paths (shown in Figure 4.4) were traversed twice to ensure repeatability of data. The results presented for each load path are the maximum of the two runs. Results are analyzed separately for each test and also compared with each other to characterize the behavior of the bridge over time.

4.2.1 Transverse Joint Behavior

The transverse UHPC joints of this bridge are of special interest due to their use in a negative moment region and the risk of opening of the interface between the UHPC and HPC precast panels as had been seen in laboratory testing (Rouse et al. 2011). As a result, the joints were heavily instrumented to help understand the performance of this type of joint. All strain values reported within this section are maximum tensile (+) strains. Compressive strains were not of concern at the transverse joint due to the superior strength of the UHPC in compression.

4.2.1.1 2011 Test

The maximum live load strains of the north and south lines of instrumentation of surface-mounted (top and bottom of deck) and embedded strain transducers for each load path from the 2011 test at the transverse joint are presented in Table 4.3 through Table 4.5.

Table 4.3. 2011 Maximum live load strains ($\mu\epsilon$) of top of deck surface-mounted gauges at transverse joint

	Load Path					
	1	2	3	4	5	6
ToD S 1	8	23	26	26	18	< 5
ToD S 2	7	22	25	26	18	< 5
ToD S 3	8	26	30	31	21	6
ToD S 4	6	20	23	24	16	< 5
ToD S 5	6	21	24	25	17	< 5
ToD N 1	14	24	23	18	9	< 5
ToD N 2	29	73	72	49	21	< 5
ToD N 3	7	12	11	9	< 5	< 5
ToD N 4	21	72	72	45	17	< 5
ToD N 5	14	26	23	17	11	< 5

Table 4.4. 2011 Maximum live load strains ($\mu\epsilon$) of bottom of deck surface-mounted gauges at transverse joint

	Load Path					
	1	2	3	4	5	6
BoD S 2	< 5	7	8	8	8	< 5
BoD S 3	< 5	< 5	< 5	< 5	< 5	< 5
BoD S 4	< 5	6	6	7	7	< 5
BoD N 2	9	18	20	19	14	< 5
BoD N 3	< 5	< 5	< 5	< 5	< 5	< 5
BoD N 4	< 5	< 5	< 5	7	8	< 5

Table 4.5. 2011 Maximum live load strains ($\mu\epsilon$) of embedded gauges at transverse joint

	Load Path					
	1	2	3	4	5	6
S2-1-3T	< 5	13	14	13	9	< 5
S2-1-2T	< 5	13	17	14	10	< 5
S2-1-1T	7	16	20	19	11	6
S1-1-1T	6	15	17	17	10	< 5
S1-1-2T	< 5	14	15	15	8	< 5
S1-1-3T	< 5	9	11	12	7	< 5
S2-3-3T	< 5	13	13	11	< 5	< 5
S2-3-2T	Corrupt	Corrupt	Corrupt	Corrupt	Corrupt	Corrupt
S1-3-1T	9	20	23	12	10	< 5
S1-3-2T	7	14	13	11	6	< 5
S1-3-3T	< 5	10	10	11	< 5	< 5

Maximum strains were recorded consistently at the same transducer location along north and south lines for both the top and bottom of the deck as well as the embedded gauges. These values are noted in the tables in boldface type. Also, note in the tables that the dotted lines separate the north and south lines of instrumentation. The notation of Corrupt signifies flawed data being reported from the transducer.

Representative data sets for the surface-mounted gauges can be seen in Figure 4.7 through Figure 4.10, which show data from load path 3 where many maximum strain values were recorded.

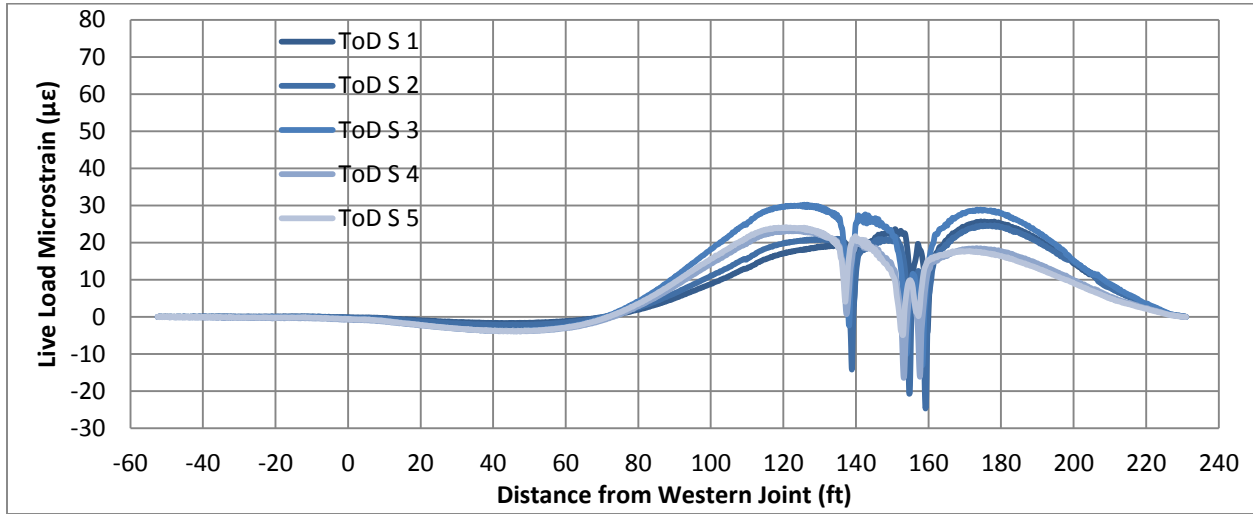


Figure 4.7. Representative data from load path 3 of 2011 live load strains of top of deck gauges south line

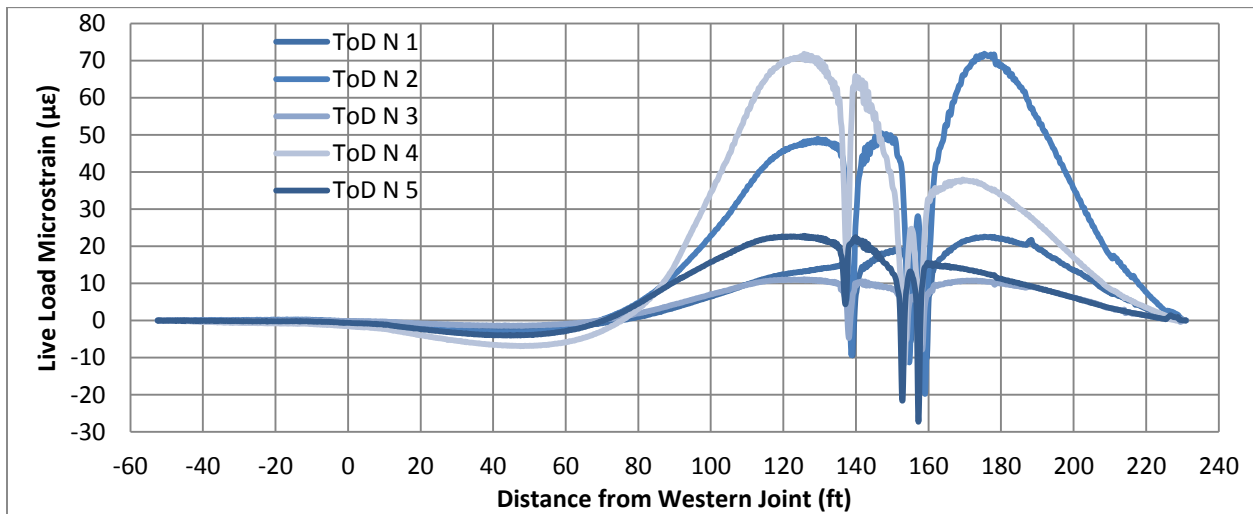


Figure 4.8. Representative data from load path 3 of 2011 live load strains of top of deck gauges north line

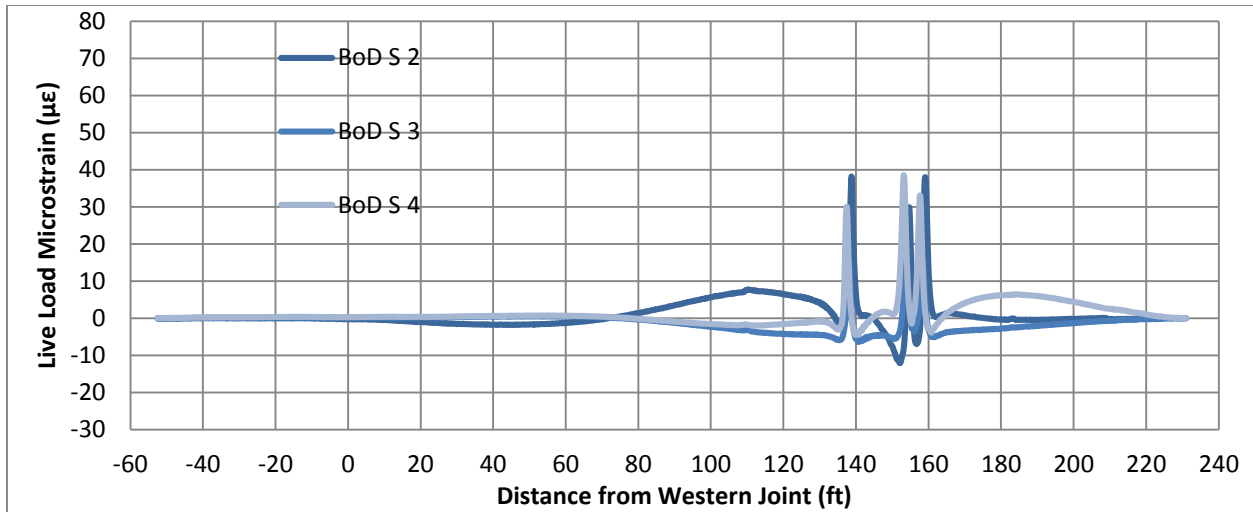


Figure 4.9. Representative data from load path 3 of 2011 live load strains of bottom of deck gauges south line

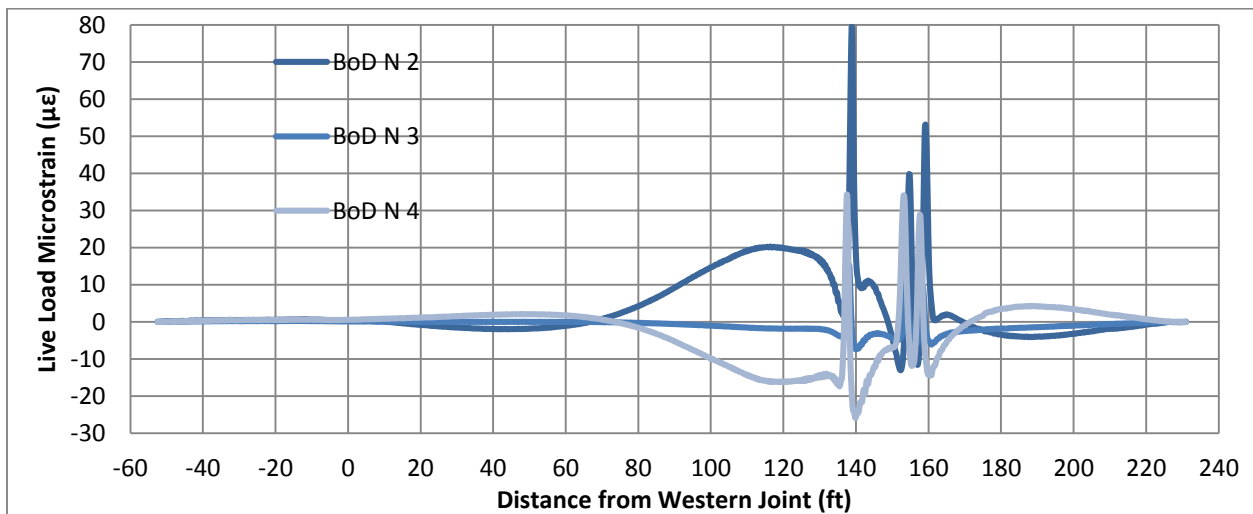


Figure 4.10. Representative data from load path 3 of 2011 live load strains of bottom of deck gauges north line

For the transverse joint location, the maximum strains for each load path occur when the truck is either approaching or exiting the east pier (~140 ft from the western joint). The maxima of these values were +73 and +72 µε, which were recorded while the truck ran along load paths 2 and 3, respectively (the paths closest to the instrumented module).

All strain values recorded at the instrumented module for gauges outside the joint and across the interface are well below the cracking strain for the HPC (~132 µε) while gauges at the centerline of the joint are well below the cracking strain for the UHPC (~250 µε). These results imply no cracking of the concrete.

There is a distinct difference in the behavior between the north and south lines of the surface-mounted gauges. Reviewing the results from the gauges mounted on the top of the deck along the south instrumentation line, all recorded strain values were very similar throughout the test with maximum strain values being recorded by the transducer located at the centerline of the UHPC joint, which is to be expected. This can be seen in Figure 4.7.

For the north line of gauges on the top of the deck, much greater maximum strain values were recorded consistently by the transducers spanning the interface between the HPC precast deck panels and the transverse UHPC joint. Figure 4.8 also shows that these interface gauges are reading significantly higher strains than adjacent gauges along the same north line.

Similar behavior was found in the gauges attached to the bottom of the deck in that there are noticeably higher strains recorded in the north line of gauges as can be seen when comparing Figure 4.9 and Figure 4.10. This could imply failure to fully develop a bond between the UHPC and HPC consistently throughout the transverse joint as was seen in the laboratory testing.

Although the location of maximum strain is at the interface for the north line of gauges, the strain value is still well below the cracking strain of the HPC and, upon visual inspection, no cracks were observed. Therefore, opening of the interface between the UHPC and HPC was not of concern at the time of the first test, but was inspected closely through comparison to the second test.

4.2.1.2 2012 Test and Comparison

The maximum live load strains from the north and south lines of surface-mounted (top and bottom of deck) and embedded strain transducers for each load path from the 2012 test at the transverse joint are presented in Table 4.6 through Table 4.8.

Table 4.6. 2012 Normalized maximum live load strains ($\mu\epsilon$) of top of deck surface-mounted gauges at transverse joint

	Load Path					
	1	2	3	4	5	6
ToD S 1	9	30	34	33	21	< 5
ToD S 2	9	32	40	41	27	6
ToD S 3	7	20	23	23	15	< 5
ToD S 4	9	32	44	48	32	6
ToD S 5	8	25	26	26	17	< 5
ToD N 1	9	15	21	10	< 5	< 5
ToD N 2	43	106	99	84	44	8
ToD N 3	10	17	14	12	6	< 5
ToD N 4	38	94	95	76	38	6
ToD N 5	16	30	29	22	12	< 5

Table 4.7. 2012 Normalized maximum live load strains ($\mu\epsilon$) of bottom of deck surface-mounted gauges at transverse joint

	Load Path					
	1	2	3	4	5	6
BoD S 2	18	43	47	43	31	11
BoD S 3	< 5	< 5	< 5	< 5	< 5	< 5
BoD S 4	12	25	26	24	17	7
BoD N 2	18	40	41	36	24	6
BoD N 3	< 5	< 5	< 5	< 5	< 5	< 5
BoD N 4	9	11	10	9	8	< 5

Table 4.8. 2012 Normalized maximum live load strains ($\mu\epsilon$) of embedded gauges at transverse joint

	Load Path					
	1	2	3	4	5	6
S2-1-3T	10	16	18	15	11	< 5
S2-1-2T	10	18	18	18	13	8
S2-1-1T	13	22	26	25	19	12
S1-1-1T	11	20	22	22	18	10
S1-1-2T	Corrupt	Corrupt	Corrupt	Corrupt	Corrupt	Corrupt
S1-1-3T	Corrupt	Corrupt	Corrupt	Corrupt	Corrupt	Corrupt
S2-3-3T	10	16	16	14	11	< 5
S2-3-2T	13	19	18	16	11	< 5
S1-3-1T	15	26	26	22	14	10
S1-3-2T	Corrupt	Corrupt	Corrupt	Corrupt	Corrupt	Corrupt
S1-3-3T	10	16	13	10	8	< 5

Like the 2011 test, maximum strains were recorded consistently at the same transducer location along north and south lines for both the top and bottom of the deck as well as the embedded gauges. The maximum tensile strain recorded in the 2012 test is $\sim 106 \mu\epsilon$, recorded by a transducer spanning the HPC/UHPC interface on the top of the deck during a run of load path 2, noticeably higher than any strain seen in the 2011 test.

A review of the data from the 2012 test indicates a distinct difference in the behavior of the transverse joint between the north and south lines of instrumentation. The difference is especially true on the top of the deck. Noticeably greater strains are still being observed across the joint interface along the north line compared to the south line as was seen in the 2011 test.

There also seems to be a consistent increase in maximum strain values between the 2011 and 2012 test with almost all maximum strains now being found at the HPC/UHPC interface locations. The most drastic increases in strains seem to be occurring at these interface locations

as can be seen by investigating the representative data from load path 2 of both tests as shown in Figure 4.11 and Figure 4.12.

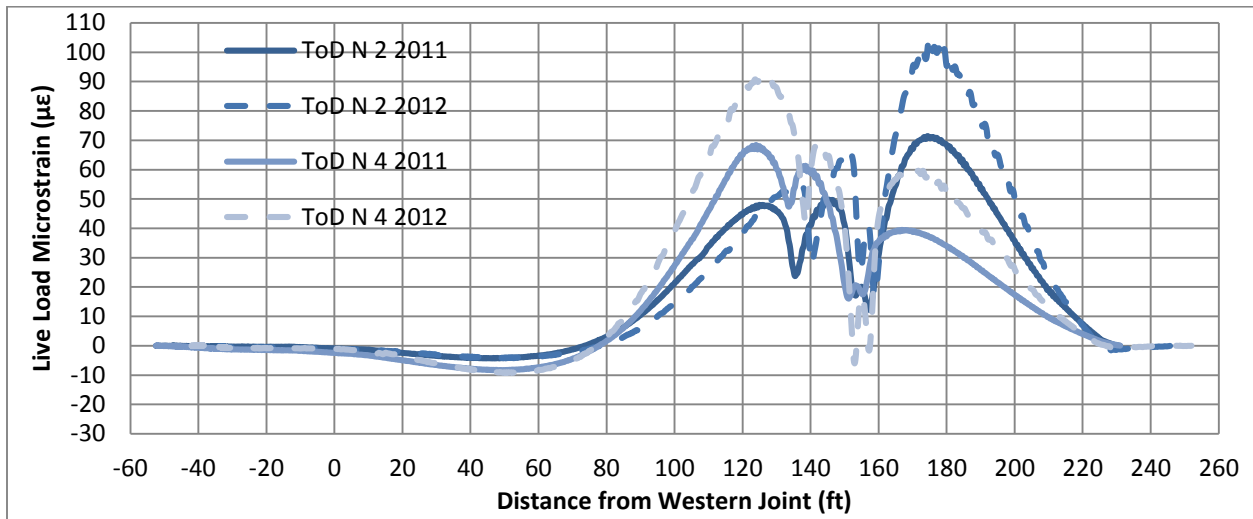


Figure 4.11. Comparison of live load strains from 2011 to 2012 of surface-mounted transducers spanning interface load path 2

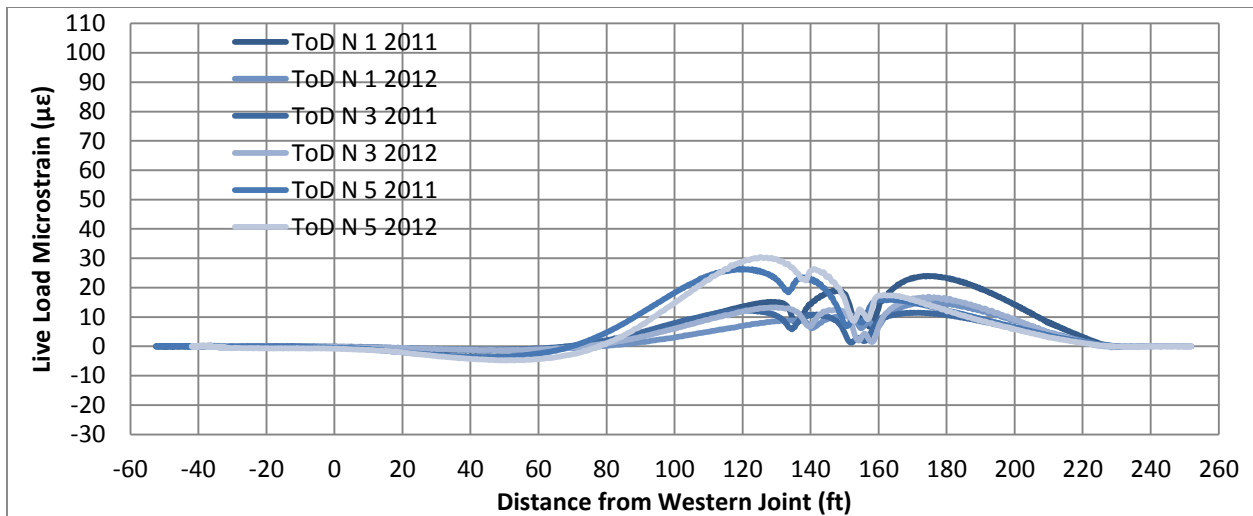


Figure 4.12. Comparison of live load strains from 2011 to 2012 of surface-mounted transducers away from interface load path 2

It is very noticeable that greater increases in tensile strains are occurring at the gauges spanning the interface of the HPC/UHPC as shown in **Error! Not a valid bookmark self-reference..**

Table 4.9. Live load strain difference from 2011 test to 2012 test top of deck transducers load path 2

	Transducer				
	ToD N 1	ToD N 2	ToD N 3	ToD N 4	ToD N 5
2011 LL Strain ($\mu\epsilon$)	24	71	12	68	26
2012 LL Strain ($\mu\epsilon$)	15	103	17	92	30
Difference ($\mu\epsilon$)	-9	+32	+4	+24	+4

The general pattern of larger increases in strain at the gauges spanning the interface is seen throughout all datasets for all load paths along north and south lines on the top and bottom of the deck.

A couple of things could cause the increase in strain from test to test. One explanation could be a relaxation of the post-tensioning utilized across the transverse joint. However, this scenario is not supported by the collected data. A decrease in compressive force from the post-tensioning rods would result in a significant increase in tensile strains for all gauges at the transverse joint, not only the gauges spanning the interface. Therefore, the increase of tensile strain from test to test is much more likely explained by a breaking down of the bond between the UHPC and HPC at the joint interface, which would localize the larger increases in strain to the joint interface as seen in the data.

As recorded strain values have increased between the 2011 and 2012 test, the maximum tensile strains of the 2012 test ($\sim 106 \mu\epsilon$) have gotten much closer to the cracking strain of the HPC ($\sim 132 \mu\epsilon$). Upon visual inspection, many cracks were noticed on the top of the deck. A large majority of these cracks were noticed at the interface between the UHPC joints (both longitudinal and transverse) and the precast HPC deck modules.

The photos in Figure 4.13 through Figure 4.16 were taken at the time of the second test in May 2012 showing cracking along the joint interfaces and leakage through the bridge deck.



Figure 4.13. Observed cracking at instrumented joint at location of ToD N 4 transducer

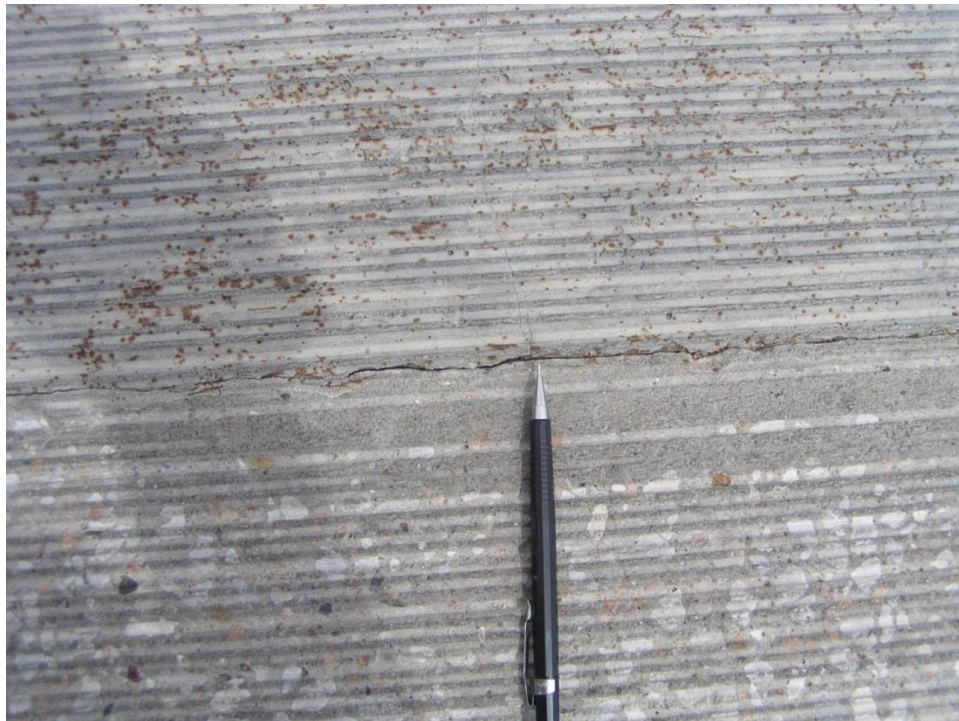


Figure 4.14. Observed cracking of longitudinal joint between modules 2 and 3



Figure 4.15. Observed efflorescence between modules 2 and 3 on bottom of deck



Figure 4.16. Close-up of cracking and efflorescence observed between modules 2 and 3 on bottom of deck

4.2.2 Girder Behavior

The following tables present the maximum values of strain recorded on the steel girders at different locations (midspan, abutment, and pier) by gauges mounted on the underside of both the top and bottom flanges of the respective beams. The reported values represent the greatest absolute value of strain seen for that location, whether tensile (+) or compressive (-). All girders were instrumented at midspan of the east end span while only girders comprising modules 1 and 3 were instrumented at the abutment and pier.

4.2.2.1 2011 Test

4.2.2.1.1 Strains at Midspan

The steel girders of the east end span were instrumented at the midspan location to investigate global flexural response of the bridge and also to calculate load fractions and distribution factors for the separate modules. Maximum strains of the midspan bottom and top flange gauges are presented in Table 4.10 and Table 4.11.

Table 4.10. 2011 Maximum live load strains ($\mu\epsilon$) of bottom flange of steel girders at midspan

	Load Path					
	1	2	3	4	5	6
M1 Mid BN	72	18	11	< 10	< 10	< 10
M1 Mid BS	89	38	25	16	< 10	< 10
M2 Mid BN	98	64	48	32	13	< 10
M2 Mid BS	62	86	69	48	21	< 10
M3 Mid BN	49	104	102	77	36	< 10
M3 Mid BS	28	93	107	105	64	16
M4 Mid BN	17	64	84	103	87	26
M4 Mid BS	< 10	39	51	80	104	47
M5 Mid BN	< 10	25	35	58	104	65
M5 Mid BS	< 10	12	17	30	62	93
M6 Mid BN	< 10	< 10	< 10	18	44	106
M6 Mid BS	< 10	< 10	< 10	< 10	17	76

Table 4.11. 2011 Maximum live load strains ($\mu\epsilon$) of top flange of steel girders at midspan

	Load Path					
	1	2	3	4	5	6
M1 Mid TN	23	< 10	< 10	< 10	< 10	< 10
M1 Mid TS	24	< 10	< 10	< 10	< 10	< 10
M2 Mid TN	43	18	< 10	< 10	< 10	< 10
M2 Mid TS	27	31	< 10	< 10	< 10	< 10
M3 Mid TN	< 10	27	27	21	< 10	< 10
M3 Mid TS	< 10	28	23	28	< 10	< 10
M4 Mid TN	< 10	< 10	< 10	41	36	< 10
M4 Mid TS	< 10	< 10	< 10	25	31	< 10
M5 Mid TN	< 10	< 10	< 10	< 10	29	16
M5 Mid TS	< 10	< 10	< 10	< 10	< 10	30
M6 Mid TN	< 10	< 10	< 10	< 10	< 10	31
M6 Mid TS	< 10	< 10	< 10	< 10	< 10	28

Maximum strain values for each load path were recorded as tensile strains in the girders located most directly underneath the specified load path as the truck was passing over the midspan location (directly over the gauges) in the bottom flange. All recorded maximum strain values from steel girders at midspan fell well below the yield strain of ASTM A709 Grade 50W steel with the greatest of these being 107 $\mu\epsilon$, which was recorded while the truck passed over the bridge along load path 3 by the transducer located on the bottom flange of the southern girder of module 3.

Two representative samples of data are presented in Figure 4.17 and Figure 4.18 showing the response of the girders both directly under and those farther away from a specified load path (load path 4).

There are obvious signs of continuity between spans. As the truck passes over the East pier (at ~140 ft), the strain values in the bottom flange of the girders switch from compressive strain (-) to a tensile strain (+) for all girders, indicating continuity between spans for live load.

The results also show a difference in strain response between the more heavily loaded girders and the girders farther away from the load path, while the test truck is on the east end span. For girders farther away from the load path, strain values recorded in the bottom flange are tensile strains while strains in the top flange are recorded as compressive strains, indicating the neutral axis is located somewhere within the steel beam.

For modules 1 and 2 the neutral axis is typically calculated between 24 and 29 in. from the underside of the bottom flange of the steel girders which are W30X99 steel beams having a depth of 29.65 in. For the girders underneath the load path, transducers on both the bottom and top flange are recording tensile strains, indicating a neutral axis above the top flange.

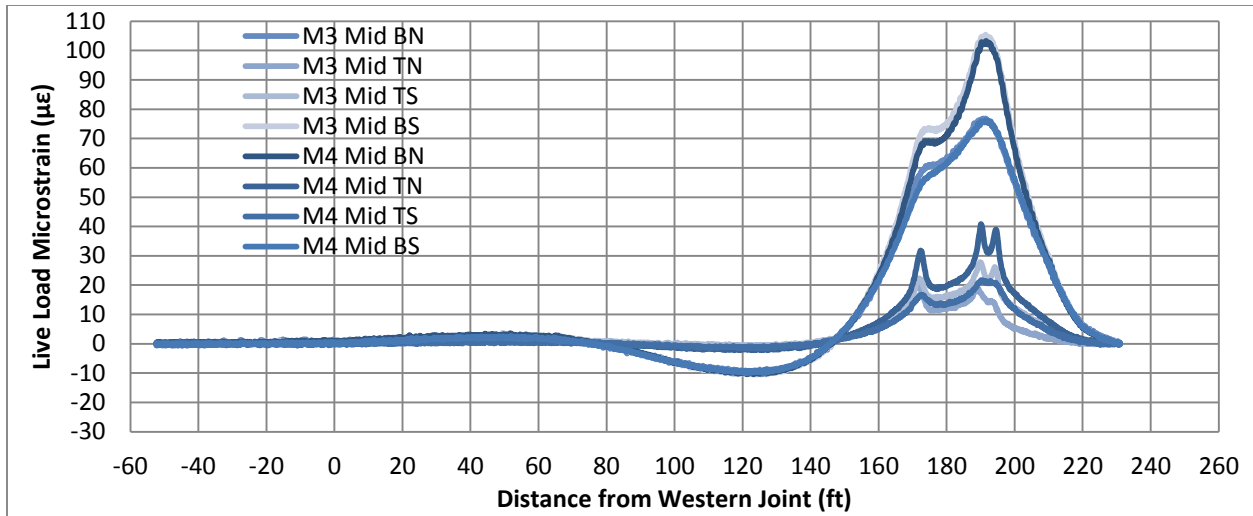


Figure 4.17. Representative data from load path 4 of 2011 live load strains for steel girders of modules 3 and 4 at midspan

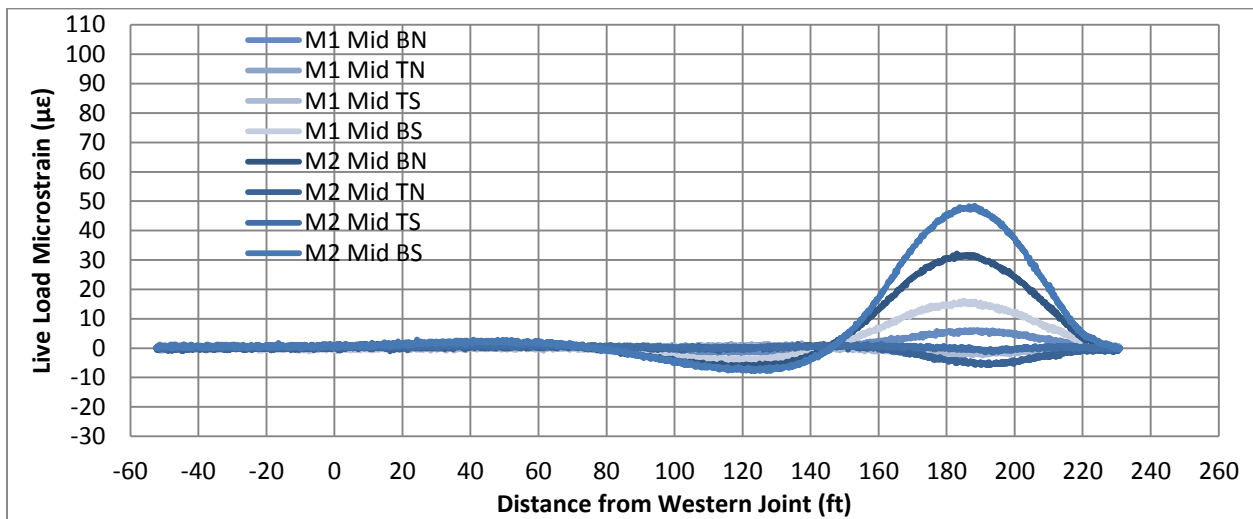


Figure 4.18. Representative data from load path 4 of 2011 live load strains for steel girders of modules 1 and 2 at midspan

These results are not necessarily unexpected due to the precast deck panels being compositely constructed with the steel girders, but the extent to which the neutral axis is above the steel girders is unexpected. At the extreme, the neutral axis is calculated to even exceed the height of the precast deck by as much as 10 in. (This is discussed further later in this report.)

As stated previously, strains recorded at the midspan of the steel girders were also used to calculate load fractions and distribution factors for the bridge. A load fraction is defined as the fraction of the total load supported by an individual element, for a given load path. Load fractions were calculated based on the assumption all girders are of equal stiffness. The load fraction for any given path can be calculated using either strains or deflections. For this test, strain values and equation (1) were used to calculate load fractions:

$$LF_i = \frac{\varepsilon_i}{\sum_{i=1}^n \varepsilon_i} \quad (1)$$

where LF_i = load fraction of the i th girder, ε_i = strain i th girder, $\sum \varepsilon_i$ = sum of all girder strains, and n = number of girders.

Using load fractions, a distribution factor can also be estimated. A distribution factor is the fraction of the total load that a girder must be designed to support when all lanes are loaded to produce maximum effects on the element. For girders 1 through 4, paths 1 and 2 were used creating the maximum effects for the north half of the bridge. For girders 5 through 8, paths 2 and 5 were used creating the maximum effects over the centerline of the bridge. For girders 9 through 12, paths 5 and 6 were used creating the maximum effects for the south half of the bridge. Therefore, the distribution factor for each girder can be expressed by equation (2):

$$DF_i = LF_{ij} + LF_{ik} \quad (2)$$

where DF_i = distribution factor of the i th girder, LF_{ij} = load fraction from path j of the i th girder, LF_{ik} = load fraction from path k of the i th girder.

Distribution factors for individual modules can be calculated simply by adding together the distribution factors for the girders comprising the specified module. Load fractions and distribution factors of both individual girders and modules for the 2011 test are presented in Table 4.12.

Table 4.12. 2011 Load fractions and distribution factors

	Module 1		Module 2		Module 3		Module 4		Module 5		Module 6	
	N	S	N	S	N	S	N	S	N	S	N	S
Girder Number	1	2	3	4	5	6	7	8	9	10	11	12
LF Path 1	0.18	0.18	0.19	0.14	0.13	0.09	0.05	0.03	0.01	0.00	0.00	0.00
LF Path 2	0.03	0.08	0.13	0.13	0.16	0.15	0.12	0.09	0.06	0.03	0.01	0.01
LF Path 3	0.02	0.06	0.11	0.12	0.15	0.16	0.13	0.10	0.08	0.04	0.02	0.01
LF Path 4	0.01	0.03	0.07	0.10	0.13	0.15	0.15	0.13	0.12	0.06	0.04	0.01
LF Path 5	0.01	0.01	0.03	0.05	0.08	0.13	0.14	0.16	0.16	0.11	0.09	0.03
LF Path 6	0.00	0.00	0.00	0.01	0.02	0.04	0.08	0.13	0.16	0.18	0.21	0.17
DF (girders)	0.21	0.26	0.32	0.27	0.24	0.28	0.26	0.25	0.32	0.29	0.30	0.20
DF (modules)	0.47		0.59		0.52		0.51		0.61		0.50	

4.2.2.1.2 Strains at Abutment and Pier

Top and bottom flanges of the steel girders under modules 1 and 3 were instrumented at the abutment and pier to investigate flexural response of the bridge and attempt to quantify end restraint of the east end span. Maximum strains of the bottom flanges of the instrumented girders

at the abutment are presented in Table 4.13 while maximum strains for the bottom flanges of the instrumented girders at the pier are presented in Table 4.14.

Table 4.13. 2011 Maximum live load strains ($\mu\epsilon$) of bottom flange of steel girders at abutment

	Load Path					
	1	2	3	4	5	6
M1 Abut BN	20	13	11	< 10	< 10	< 10
M1 Abut BS	32	11	12	< 10	< 10	< 10
M3 Abut BN	< 10	28	30	17	< 10	< 10
M3 Abut BS	< 10	25	31	29	12	< 10

Table 4.14. 2011 Maximum live load strains ($\mu\epsilon$) of bottom flange of steel girders at pier

	Load Path					
	1	2	3	4	5	6
M1 Pier BN	-40	< 10	< 10	< 10	< 10	< 10
M1 Pier BS	-47	-19	-12	< 10	< 10	< 10
M3 Pier BN	-26	-58	-56	-39	-18	< 10
M3 Pier BS	-13	-49	-59	-57	-37	< 10

For gauges located at the abutment, maximum strains were recorded as tensile strains in the girders closest to the specified load path after the front axle of the truck had exited off of the bridge while the rear axle was still on the east end span. These maxima were seen in the bottom flange registering just over +30 $\mu\epsilon$. Another local maximum occurs as the test truck is near the midspan of the east end span. When the test truck is located at this position, the bottom flange of the girders at the abutment registers compressive strains indicating a negative moment at the abutment as expected due to the semi-integral abutments. Strains recorded in the top flange of the girders at the abutment never registered above 10 $\mu\epsilon$, tensile or compressive.

A representative data set is shown in Figure 4.19 for gauges mounted to the girders under module 3 at the abutment for load path 3 showing this behavior. Due to the stopping of data collection in the 2011 test immediately after the rear axle passed the east joint, full behavior of the semi-integral abutment was not able to be seen, but is discussed in greater detail in the subsequent section related to the 2012 test data.

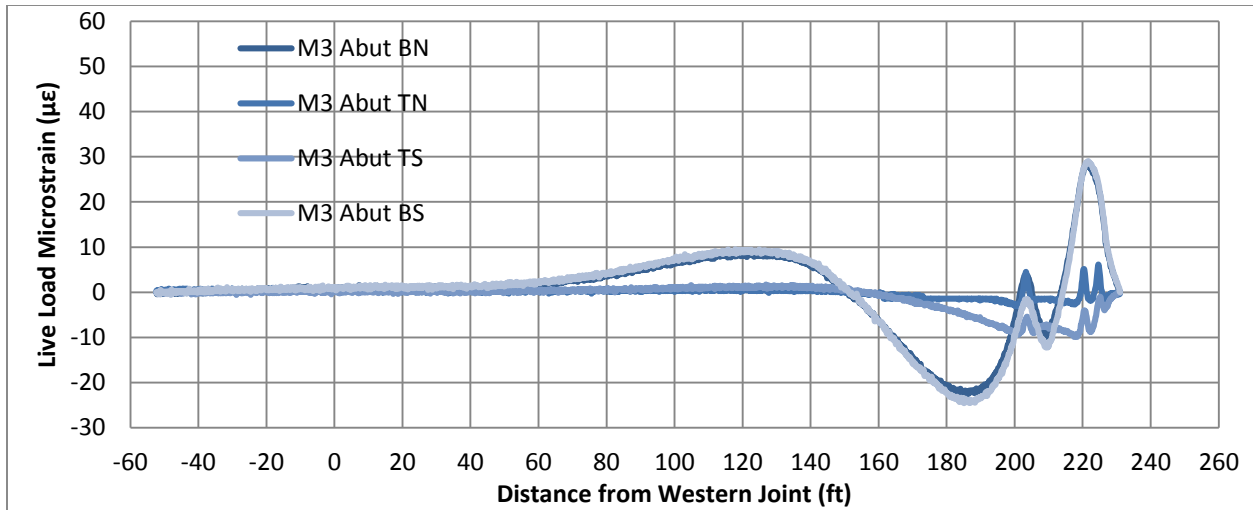


Figure 4.19. Representative data from load path 3 of 2011 live load strains for steel girders of module 3 at abutment

For gauges located at the pier, maximum strains were recorded as compressive strains in the bottom flange of the girder closest to the specified load path as the truck approached the pier from the west. Compressive strains in the bottom flange imply a negative moment region at the pier. This is to be expected based on the fact that the bridge was designed to be continuous for live loads. The greatest strains recorded in the top flange of the girders at the pier location never registered above 10 $\mu\epsilon$, tensile or compressive. A representative sample of these data from load path 3 is shown in Figure 4.20.

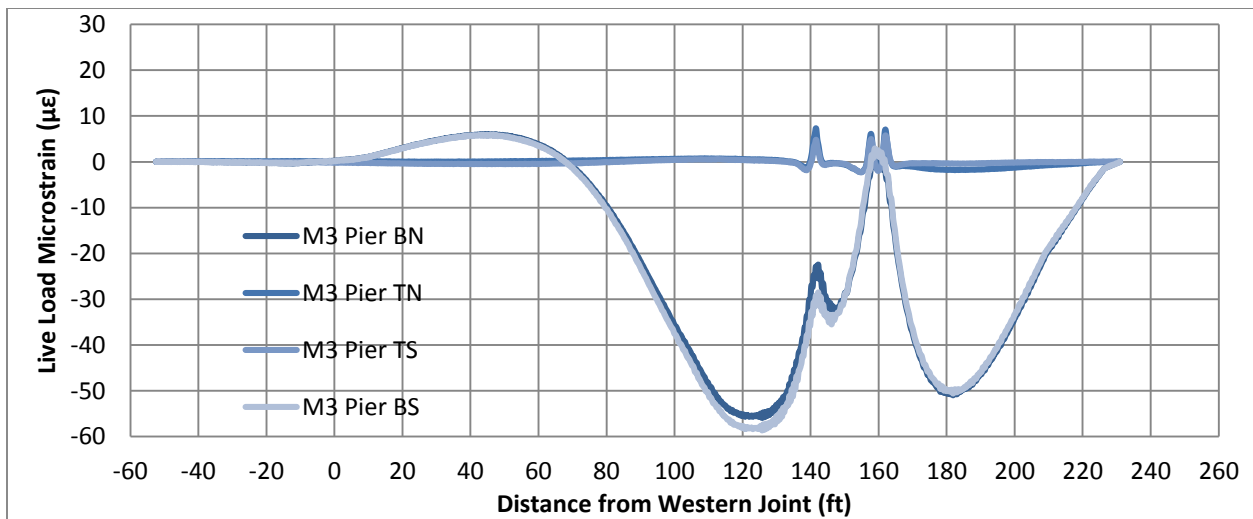


Figure 4.20. Representative data from load path 3 of 2011 live load strains for steel girders of module 3 at pier

4.2.2.2 2012 Test and Comparison

4.2.2.2.1 Strains and Differential Deflections at Midspan

Maximum live load strains recorded at the midspan of the steel girders in the 2012 test are presented in Table 4.15 and Table 4.16.

Table 4.15. 2012 Normalized maximum live load strains ($\mu\epsilon$) of bottom flange of steel girders at midspan

	Load Path					
	1	2	3	4	5	6
M1 Mid BN	75	18	11	< 10	< 10	< 10
M1 Mid BS	78	33	24	14	< 10	< 10
M2 Mid BN	97	63	47	29	11	< 10
M2 Mid BS	67	99	80	53	23	< 10
M3 Mid BN	52	115	113	83	40	< 10
M3 Mid BS	25	85	99	99	58	14
M4 Mid BN	16	60	87	100	84	24
M4 Mid BS	< 10	38	56	76	102	44
M5 Mid BN	< 10	25	39	54	99	64
M5 Mid BS	< 10	12	20	29	61	89
M6 Mid BN	< 10	< 10	12	17	43	99
M6 Mid BS	< 10	< 10	< 10	< 10	20	83

Table 4.16. 2012 Normalized maximum live load strains ($\mu\epsilon$) of top flange of steel girders at midspan

	Load Path					
	1	2	3	4	5	6
M1 Mid TN	24	< 10	< 10	< 10	< 10	< 10
M1 Mid TS	22	< 10	< 10	< 10	< 10	< 10
M2 Mid TN	45	17	< 10	< 10	< 10	< 10
M2 Mid TS	12	14	< 10	< 10	< 10	< 10
M3 Mid TN	< 10	36	38	26	< 10	< 10
M3 Mid TS	< 10	25	24	27	< 10	< 10
M4 Mid TN	< 10	< 10	11	33	29	< 10
M4 Mid TS	< 10	< 10	< 10	13	19	< 10
M5 Mid TN	< 10	< 10	< 10	< 10	16	12
M5 Mid TS	< 10	< 10	< 10	< 10	< 10	21
M6 Mid TN	< 10	< 10	< 10	< 10	< 10	34
M6 Mid TS	< 10	< 10	< 10	< 10	< 10	24

Maximum strain values of the steel girders at midspan for the 2012 test were very similar to those measured during the first test. The maximum tensile strains were again seen in the bottom flange of the girders located most directly underneath the specified load path while the truck was passing over midspan of the east end span. The greatest strain seen in the midspan girders during the 2012 test was $\sim 115 \mu\epsilon$ during load path 2 in the bottom flange of the north girder under module 3, just slightly larger than the maximum strain seen in the 2011 test ($\sim 107 \mu\epsilon$).

Maximum differential deflections between the HPC precast deck and longitudinal UHPC joint were also investigated in the 2012 test. Deflections were recorded between deck of module 4 and longitudinal joint at the centerline of the bridge at the midspan location of the east end span. Maximum differential deflections for each load path are presented in Table 4.17. The greatest recorded deflection was 0.004 in., or essentially zero.

Table 4.17. 2012 Maximum differential deflection at midspan

	Load Path					
	1	2	3	4	5	6
Deflection (in.)	0.003	.004	.004	.004	.004	.004

Figure 4.21 and Figure 4.22 show comparisons of representative samples of data between the 2011 and 2012 test for module 3 strains recorded in the top and bottom flanges for load path 4. The differences between the tests are then quantified in

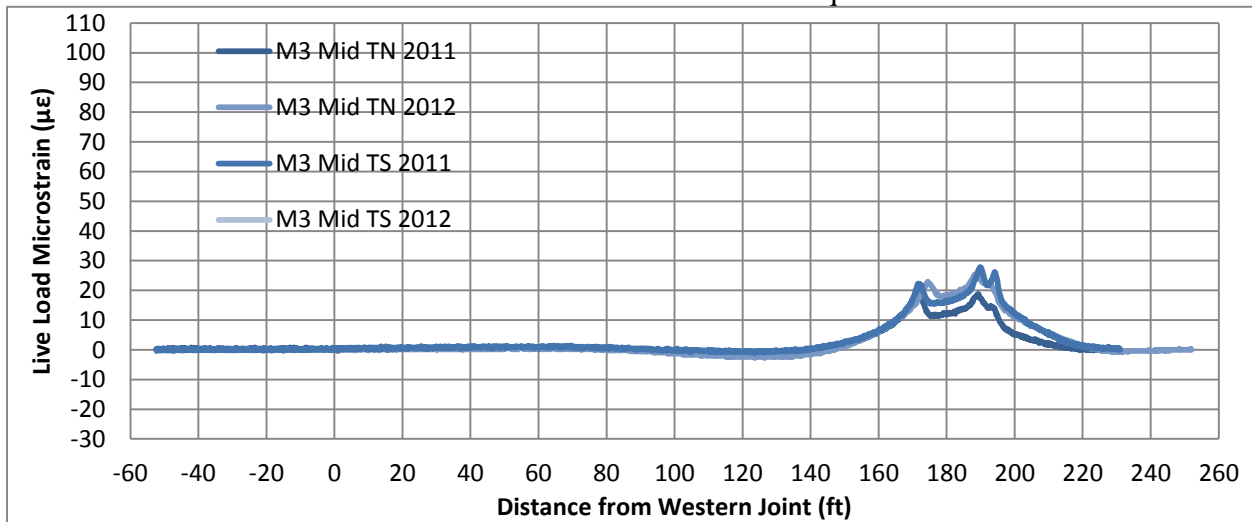


Figure 4.22. Comparison of live load strains from 2011 to 2012 of transducers on top flange of girder at midspan for module 3 from load path 4

Table 4.18 and Table 4.19.

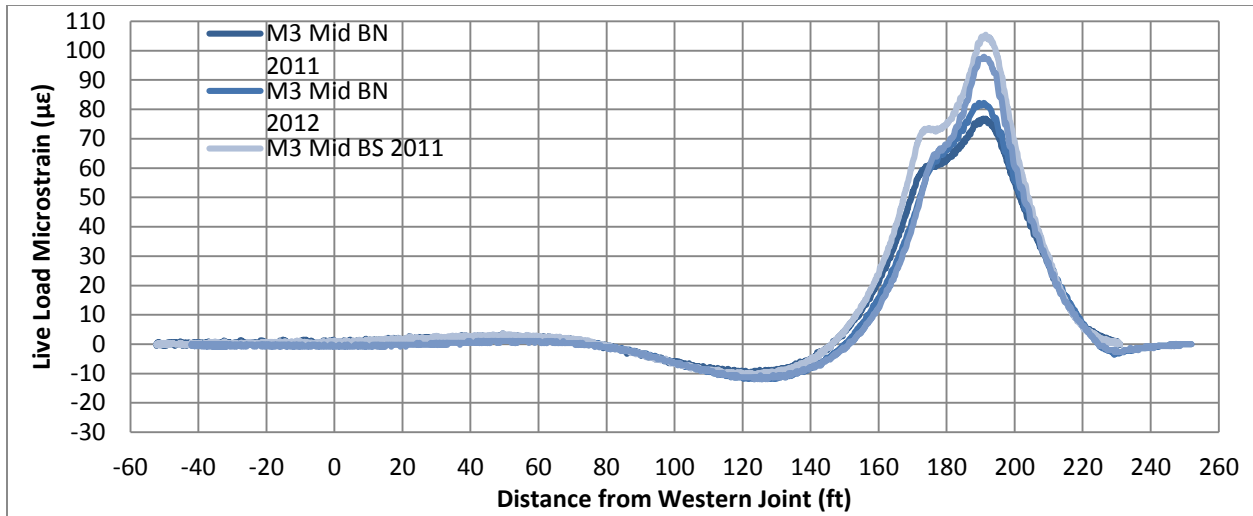


Figure 4.21 Comparison of live load strains from 2011 to 2012 of transducers on bottom flange of girder at midspan for module 3 from load path 4

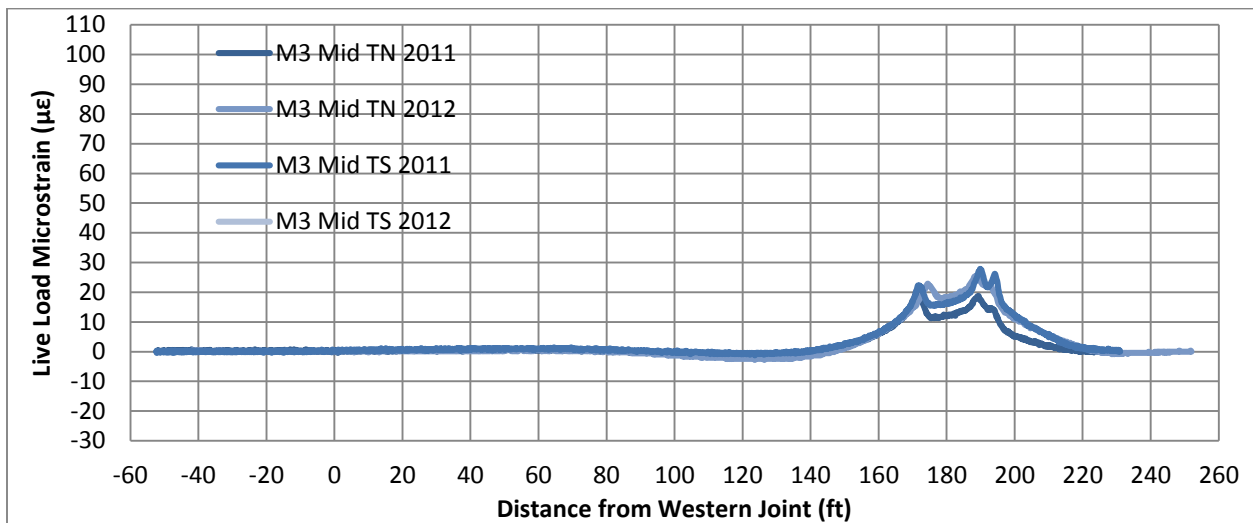


Figure 4.22. Comparison of live load strains from 2011 to 2012 of transducers on top flange of girder at midspan for module 3 from load path 4

Table 4.18. Live load strain difference from 2011 test to 2012 test of bottom flange transducer on girder at midspan for module 3 from load path 4

	Transducer	
	M3 Mid BN	M3 Mid BS
2011 LL Strain (µε)	77	106
2012 LL Strain (µε)	82	98
Difference (µε)	+5	-8

Table 4.19. Live load strain difference from 2011 test to 2012 test of top flange transducer on girder at midspan for module 3 from load path 4

	Transducer	
	M3 Mid TN	M3 Mid TS
2011 LL Strain ($\mu\epsilon$)	21	28
2012 LL Strain ($\mu\epsilon$)	26	27
Difference ($\mu\epsilon$)	+5	-1

Continuity is still seen in the 2012 test as is shown by the strain reversal as the truck moves from the center span to the east end span. It can be seen that the differences between tests are very small with differences consistently less than 10 $\mu\epsilon$. There is also not necessarily a trend of constantly increasing or constantly decreasing strain between the 2011 and 2012 test, indicating that the difference in strain values between tests could likely be attributed to instrumentation accuracy, slight difference in position of gauges, etc. as opposed to changes in bridge behavior.

For the heavily-loaded girders underneath the specified load paths, neutral axis locations are again calculated to be above the deck. There are a couple of possible explanations for this occurrence. One is that there is an added axial force within the girders causing a shift in the recorded strains of both the top and bottom flanges (which would result in the neutral axis appearing to be higher than expected). Another explanation could be that the integral guardrails are elevating the neutral axis of all girders along the cross-section of the bridge, although it is very unlikely that it would affect them to this degree.

Load fractions and distribution factors were again calculated for the 2012 test and then compared with those from the 2011 test. The results from the 2012 test are shown in Table 4.20. Changes in distribution factors from 2011 to 2012 are minimal and are presented in Table 4.21.

Table 4.20. 2012 Load fractions and distribution factors

	Module 1		Module 2		Module 3		Module 4		Module 5		Module 6	
	N	S	N	S	N	S	N	S	N	S	N	S
Girder Number	1	2	3	4	5	6	7	8	9	10	11	12
LF Path 1	0.20	0.16	0.18	0.18	0.09	0.08	0.06	0.03	0.01	0.01	0.00	0.00
LF Path 2	0.04	0.08	0.13	0.15	0.16	0.12	0.12	0.09	0.06	0.03	0.02	0.00
LF Path 3	0.02	0.05	0.10	0.14	0.14	0.13	0.12	0.12	0.09	0.05	0.03	0.01
LF Path 4	0.01	0.04	0.08	0.12	0.14	0.13	0.12	0.12	0.11	0.07	0.04	0.01
LF Path 5	0.00	0.01	0.03	0.07	0.10	0.12	0.13	0.14	0.13	0.12	0.10	0.05
LF Path 6	0.00	0.00	0.00	0.01	0.02	0.05	0.08	0.13	0.15	0.16	0.19	0.21
DF (girders)	0.24	0.24	0.31	0.33	0.28	0.26	0.24	0.24	0.28	0.28	0.29	0.26
DF (modules)	0.48		0.64		0.54		0.48		0.56		0.55	

Table 4.21. Comparison of 2011 and 2012 distribution factors

	Module 1	Module 2	Module 3	Module 4	Module 5	Module 6
2011 DF	0.47	0.59	0.52	0.51	0.61	0.50
2012 DF	0.48	0.64	0.54	0.48	0.56	0.55
% Difference	2.1	8.5	3.8	-5.9	-8.2	10

All calculated distribution factors for individual modules are well below the conservative lateral live load distribution factor of 1.0 used to calculate the test load levels by the bridge design engineer, HNTB.

4.2.2.2.2 Strains at Abutment

The 2012 maximum live load strain results of the top flange of the instrumented modules at the east span abutment location are presented in Table 4.22.

Table 4.22. 2012 Normalized maximum live load strains ($\mu\epsilon$) of bottom flange of steel girders at abutment

	Load Path					
	1	2	3	4	5	6
M1 Abut BN	21	15	12	< 10	< 10	< 10
M1 Abut BS	22	12	12	< 10	< 10	< 10
M3 Abut BN	< 10	-25	-22	-14	< 10	< 10
M3 Abut BS	< 10	-21	-26	-25	-11	< 10

As in the 2011 test, all strain values recorded by the transducers at the abutment are well below the yield strain of the steel girders with the greatest being -25 $\mu\epsilon$. Maximum strains recorded in the top flanges at the abutment again never registered higher than 10 $\mu\epsilon$, tensile or compressive.

Representative sets of data comparing results from the 2011 test to the 2012 test are shown in Figure 4.23.

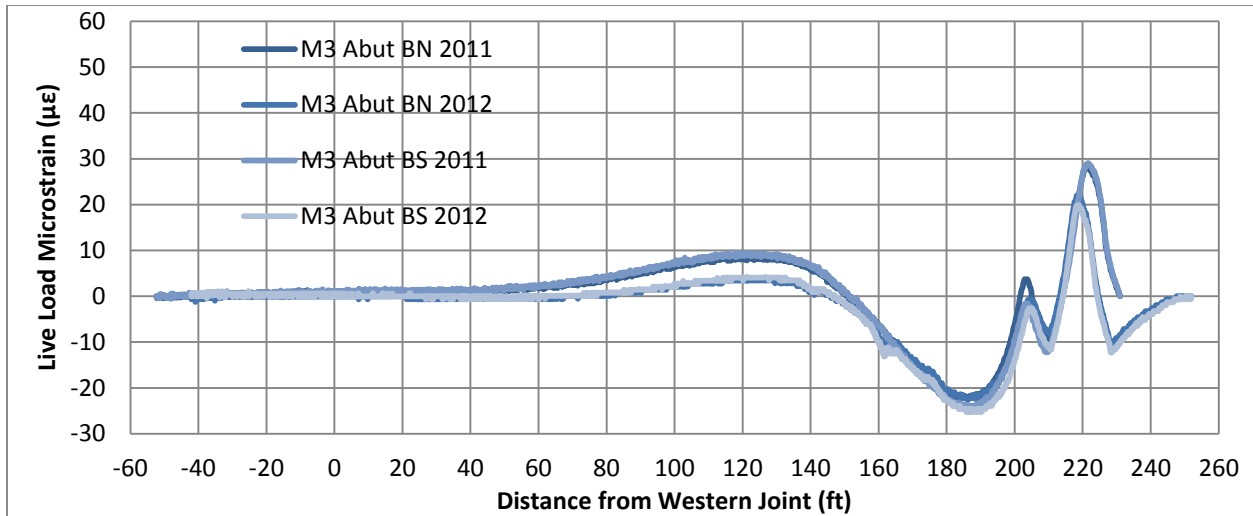


Figure 4.23. Comparison of live load strains from 2011 to 2012 of transducers on bottom flange of girder at abutment for module 3 from load path 3

In this figure, it can be seen that maximum strain values recorded in the bottom flange for a majority of the load paths have shifted from tensile in the 2011 test to compressive in the 2012 test. This is due to the fact that data stopped being collected as soon as the rear axle left the bridge span in the first test while, in the second test, data was collected until the rear axle was approximately 20 ft past the east joint. Therefore, the behavior of the semi-integral abutment was captured as the test truck exited on the approach slab in the data from the 2012 test.

After the truck exits the bridge span, compressive strains are again recorded in the bottom flange of the girders at the abutment. If data were zeroed for the second test at the same location as the first test, values would be very similar. Therefore, it is evident that continuity was maintained at the semi-integral abutment of the east end span from the first to the second test although it is difficult to say to what degree.

4.2.2.2.3 Strains at Pier

Table 4.23 presents the maximum values of the live load strains recorded in the top flanges for the 2012 test at the east pier location. Maximum strains recorded in the top flanges at the pier again never registered higher than 10 µε, tensile or compressive.

Table 4.23. 2012 Normalized maximum live load strains (µε) of bottom flange of steel girders at pier

	Load Path					
	1	2	3	4	5	6
M1 Pier BN	-42	< 10	< 10	< 10	< 10	< 10
M1 Pier BS	-46	-19	-14	< 10	< 10	< 10
M3 Pier BN	-23	-49	-46	-36	-15	< 10
M3 Pier BS	-12	-42	-50	-49	-30	< 10

Maximum strain values are still recorded as compressive strains in the bottom flange of girders closest to the specified load path as in the 2011 test, but seem to have become uniformly less compressive throughout the second test. This behavior can be seen in the representative data from load path 3 of the instrumented girder under module 3 in Figure 4.24.

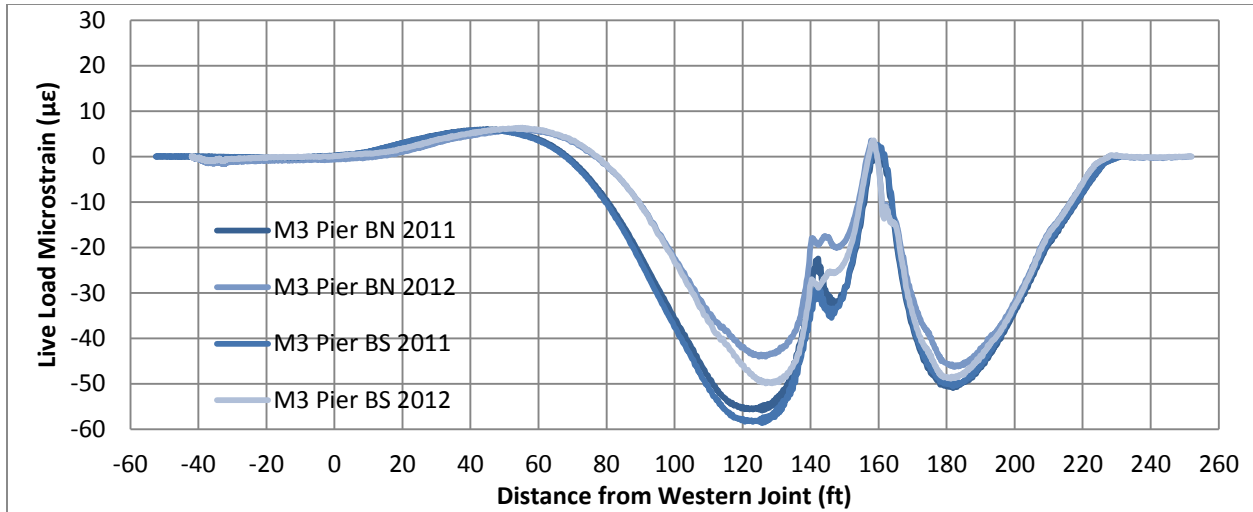


Figure 4.24. Comparison of live load strains from 2011 to 2012 of transducers on bottom flange of girder at pier for module 3 from load path 3

This loss of compressive strain shows a reduction in the magnitude of the negative moment seen at the pier. This is indicative of a loss of continuity to some degree at the east pier location and moving more toward a simply supported condition. This would also be supported by the indication of loss of bond between the precast HPC deck panels and the UHPC transverse joint as was reported previously.

4.2.3 East Pier Behavior

4.2.3.1 Pier Cap Strain Results

The east pier cap was instrumented at the centerline of the bridge on both the top and bottom with strain transducers. Using these transducers, the flexural behavior was able to be quantified and a neutral axis depth was calculated.

4.2.3.1.1 2011 Test

Maximum strains for both the top and bottom strain transducers mounted on the pier cap are presented in Table 4.24.

Table 4.24. 2011 Maximum strains of pier cap

	Load Path					
	1	2	3	4	5	6
Top ($\mu\epsilon$)	-7	-22	-25	-27	-22	-7
Bottom ($\mu\epsilon$)	35	126	150	161	131	35

Maximum tensile strains are recorded in the bottom of the pier cap during runs over load path 4 (test truck centered on bridge) as the truck passes over the east pier. Maximum compressive strains are found at the same truck location at the top of the pier cap. Recorded tensile strains on the bottom of the pier cap exceed the cracking strain of the HPC ($\sim 132 \mu\epsilon$) indicating cracking under service level loads, which would be expected. Neutral axis location was calculated using data from load path 4 and was determined to be located 56.3 in. from the bottom of the pier cap at the centerline of the bridge.

4.2.3.1.2 2012 Test and Comparison

Maximum strain values for the top and bottom strain transducers mounted on the pier cap for the 2012 test are presented in Table 4.25.

Table 4.25. 2012 Normalized maximum live load strains ($\mu\epsilon$) of pier cap

	Load Path					
	1	2	3	4	5	6
Pier Cap Top	-6	-20	-23	-24	-19	-6
Pier Cap Bottom	26	90	112	115	89	24

Maximum strain values were again found as the test truck passed over the east pier during runs for load path 4. There is a general trend in the change of strains from the 2011 test to the 2012 test. Compressive strains decrease in magnitude slightly while tensile strains decrease in magnitude a significant amount. The result of this is the neutral axis moving slightly downward toward the bottom of the pier cap. The calculated neutral axis location for the 2012 test using data from load path 4 is 54.3 in. from the bottom of the pier cap. A representative sample of data is presented in Figure 4.25, showing strain values from load path 4 of both the first and second test.

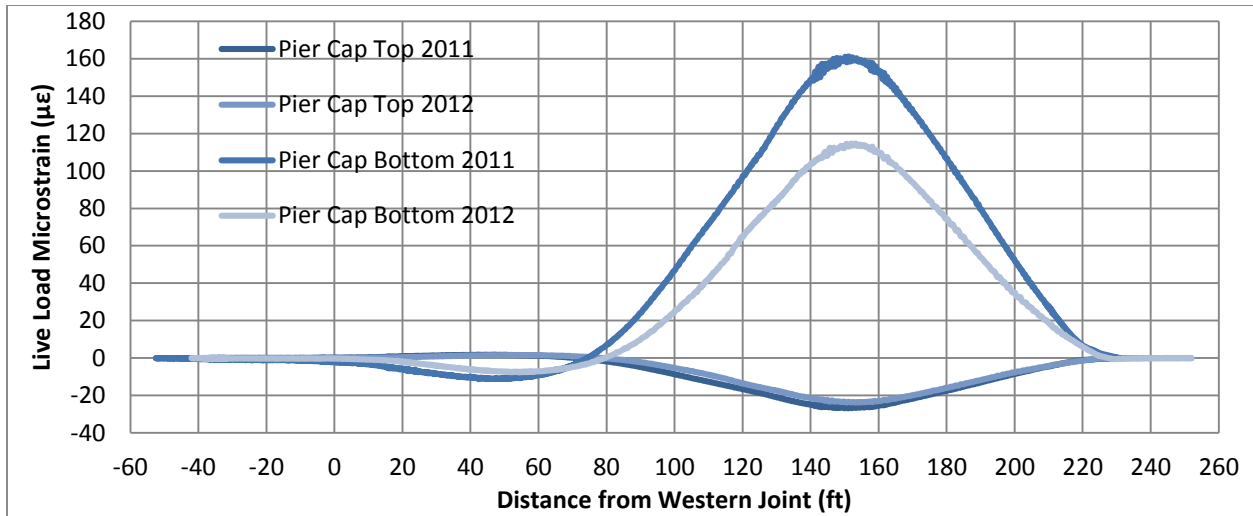


Figure 4.25. Comparison of live load strains of pier cap

The difference between tests can be explained by a couple of occurrences. First, it is possible that the transducer of the first test was located over a crack location, which would result in a greater strain value. Also, there could be strain relief occurring from the first test to the second test as a result of development of more cracks over time.

4.2.3.2 Pier Cap to Column Interface

The interface between the north column and the pier cap of the east pier was instrumented with string potentiometers in both tests to record deflections. This location was instrumented to monitor any rocking of the pier cap on its support.

In 2011, the interface was instrumented with two string potentiometers on the north face of the column/pier cap, with one on the west and one on the east, to determine rocking in the longitudinal direction. In the 2012 test, two string potentiometers were added on the south face (east and west) to identify any rocking in the transverse direction.

4.2.3.2.1 2011 Test

Maximum deflections recorded at the pier cap to column interface for the 2011 test are presented in Table 4.26. No deflection recorded at the interface exceeded 0.005 in. Therefore, the maximum differential from one side of the column to the other is 0.01 in., or effectively zero.

Table 4.26. 2011 Maximum deflections at pier cap to column interface

	Load Path					
	1	2	3	4	5	6
East (in.)	0.005	0.005	0.005	0.004	0.004	0.004
West (in.)	0.004	0.005	0.004	0.004	0.004	0.004

4.2.3.2.2 2012 Test and Comparison

Maximum deflections recorded at the pier cap to column interface for the 2012 test are presented in Table 4.27.

Table 4.27. 2012 Maximum deflections at pier cap to column interface

	Load Path					
	1	2	3	4	5	6
Northeast (in.)	0.004	0.003	0.005	0.004	0.005	0.004
Northwest (in.)	0.004	0.004	0.005	0.004	0.003	0.004
Southeast (in.)	0.002	0.002	0.002	0.002	0.002	0.002
Southwest (in.)	0.003	0.003	0.005	0.004	0.005	0.005

The results from the 2012 test reflect the same conclusion as the 2011 test, with no deflections registering greater than 0.005 in. The greatest differential again could only be 0.01 in. Therefore, there is no concern for rocking of the pier cap on the column in either the transverse or the longitudinal direction.

5 CONCLUSIONS

The use of moment-resisting transverse UHPC joints at pier locations in the Keg Creek Bridge was a first for the US and is one of many concepts being employed to reduce road closure time as part of the development of ABC practices to be used throughout the country. As the bridge was being designed, simultaneous laboratory testing was being performed at Iowa State University of these transverse joints to be used. The results of these tests indicated special attention needed to be paid at these locations due to insufficient bond strength between the HPC and UHPC.

Through further laboratory testing of the bond strength at the HPC/UHPC interface presented in this report, it is clear that there was cause for concern of opening at these interfaces. These concerns were reinforced by the findings in the comparison of the live load field tests. Visual inspection, as well as evaluation of the collected data, showed a breakdown of the bond between the interface of the HPC and UHPC at the joints. The breakdown of this bond resulted in cracking of the deck allowing an ingress of road salts, which is verified by the presence of efflorescence on the underside of the bridge deck at joint interfaces.

Furthermore, the live load field testing was also used to quantify and compare global bridge behavior over a period of approximately seven months. The overall behavior of the bridge was very similar from test to test with the exception of the breakdown of bond at the joint interfaces. The laboratory and live load field testing performed in relation to the Keg Creek Bridge resulted in the following conclusions.

5.1 Bond Testing

- Testing of the bond in the laboratory indicated there is virtually no bond between precast HPC and UHPC when no surface preparation is implemented at the interface.
- Considering both the direct tension test and the simulated MOR test, the most effective of the interface preparations was the use of a 3,000 psi pressure wash.
- All MOR average results fell below the estimated MOR of a 5,000 psi compressive strength HPC material (which was used in the Keg Creek Bridge), indicating the most likely location of cracking will be at the interface of the HPC and UHPC materials.
- Testing revealed a rather large variation in bond strength from sample to sample, indicating an inconsistency in bond development between the HPC and UHPC materials regardless of the interface preparation.
- UHPC maturity also affects the bond strength between the HPC and UHPC. The bond strength reaches a maximum value near the 7 day UHPC age and then decreases as the UHPC reaches the 14 and 28 day ages. This indicates a deterioration of bond over time.

5.2 Design Assumptions

- Lateral live load distribution factors for all modules were calculated to be much less than the 1.0 value used by the design engineer.
- Live load continuity between spans was verified by the strain reversal measured by the transducers mounted on the steel girders at midspan and also the negative moments seen at the east pier location.

5.3 Maximum Bridge Strains and Displacements

- The maximum recorded strains at the transverse joint away from the interface were well below the cracking strain for both the HPC and UHPC materials in both tests indicating cracking is unlikely at service level loads at these locations.
- The maximum recorded strains at the transverse joint across the interface of the HPC/UHPC were inconsistent when comparing north and south lines of instrumentation, while also being much greater than adjacent gauges along the north line. This result indicates an inconsistency in bonding of the different materials and points out a location of concern for cracking.
- The maximum recorded strains of the steel girders were significantly less than the yield strain of ASTM A709 Grade 50W steel at all instrumented locations (midspan, abutment, and pier) indicating yielding of the girders is unlikely at service level loads.
- The maximum recorded tensile strains of the pier cap in the 2011 test were greater than the cracking strain of the HPC material, which would be expected as the pier cap would be designed to crack.
- Maximum differential displacements between the HPC deck and UHPC longitudinal joint recorded in the 2012 test were effectively zero, showing no concern for excessive differential deflection.
- Maximum displacements across the interface of the pier cap to column connection of the east pier were minimal in both tests, showing no evidence for rocking of the pier cap in either the transverse or the longitudinal direction.

5.4 Comparison of 2011 and 2012 Pseudo-Static Live Load Tests

- In general, the behavior of the bridge is very similar between the 2011 and 2012 tests with the exception of strains across the interface between the HPC deck and UHPC transverse joint and strains of the steel girders at the pier.

- Maximum strains across the interface of the HPC deck and the UHPC transverse joint increased significantly between the 2011 test and 2012 test indicating a loss of bond and potential cracking, which was confirmed through visual inspection of the joint.
- Maximum compressive strains in the bottom flange of the girders at the pier see a noticeable reduction in value from the first to second test, indicating a reduction in negative moment and implying a loss of continuity, to some degree, between spans. This result would be expected with the deterioration of the bond between the HPC deck and the UHPC transverse joint.
- Neutral axis depths calculated from the strains recorded at the midspan location of the steel girders most directly underneath specified load paths resulted in neutral axes located above the elevation of the concrete deck consistently for both tests.

REFERENCES

- American Concrete Institute (ACI). 2011. *Building Code Requirements for Structural Concrete (ACI 318-11) and Commentary*. Farmington Hills: American Concrete Institute.
- Iowa DOT Office of Bridges and Structures. 2011. US 6 Bridge over Keg Creek: Project Information. <http://www.iowadot.gov/us6KegCreek/projectinfo.html>.
- Rouse, J. M., T. Wipf, B. Phares, and D. Hartwell. 2011. *Laboratory Testing of Ultra High Performance Concrete Deck Joints for Use in Accelerated Bridge Construction*. SHRP2 R04 Phase III- Task 10C Report. HNTB Corporation.

BIBLIOGRAPHY

- Iowa Department of Transportation. 2011. *Bridge Plans for US 6 Over Keg Creek in Pottawattamie County*. Iowa DOT Project No. BRF-006-1(114)-38-78.